

This document is confidential and is proprietary to the American Chemical Society and its authors. Do not copy or disclose without written permission. If you have received this item in error, notify the sender and delete all copies.

**Nafion® Induced Surface Confinement of Oxygen in Carbon Supported Oxygen Reduction Catalysts.**

Journal:	<i>The Journal of Physical Chemistry</i>
Manuscript ID	jp-2015-10162x
Manuscript Type:	Article
Date Submitted by the Author:	16-Oct-2015
Complete List of Authors:	Chlistunoff, Jerzy; Los Alamos National Laboratory, Materials Physics and Applications Division Sansiñena, Jose-Maria; LANL: Los Alamos National Laboratory, C-CDE: Chemical Diagnostics & Engineering

SCHOLARONE™  
Manuscripts

1  
2  
3  
4  
5  
6  
7 Nafion® Induced Surface Confinement of Oxygen  
8  
9  
10  
11 in Carbon Supported Oxygen Reduction Catalysts.  
12  
13  
14  
15  
16  
17  
18  
19

20 *Jerzy Chlistunoff\* and José-María Sansiñena*  
21  
22  
23  
24  
25

26 Los Alamos National Laboratory  
27  
28  
29

30 P.O. Box 1663, Los Alamos, NM 87545  
31  
32  
33  
34  
35  
36  
37  
38  
39  
40  
41  
42  
43  
44  
45  
46  
47  
48  
49  
50  
51  
52  
53  
54

55  
56 e-mail: jerzy@lanl.gov  
57  
58  
59  
60

1  
2  
3 KEYWORDS: self-assembly, graphitic, catalyst support, hydrophobicity, pyrolyzed catalysts  
4  
5  
6  
7  
8  
9  
10  
11  
12  
13  
14  
15  
16  
17  
18  
19  
20  
21  
22  
23  
24  
25  
26  
27  
28  
29  
30  
31  
32  
33  
34  
35  
36  
37  
38  
39  
40  
41  
42  
43  
44  
45  
46  
47  
48  
49  
50  
51  
52  
53  
54  
55  
56  
57  
58  
59  
60

1  
2  
3 ABSTRACT  
4  
5  
6

7 Surface confinement of oxygen inside layers of Nafion® self-assembled on carbon supported  
8 oxygen reduction reaction (ORR) catalysts was studied. It is demonstrated that oxygen  
9 accumulates in the hydrophobic component of the polymer remaining in contact with the carbon  
10 surface. The amount of surface confined oxygen increases with the degree of carbon surface  
11 graphitization, which promotes the self-assembly of the polymer. Planar macrocyclic ORR  
12 catalysts possessing a delocalized system of  $\pi$  electrons such as Co and Fe porphyrins and  
13 phthalocyanines have virtually no effect on the surface confinement of oxygen, in accordance with  
14 their structural similarity to graphitic carbon surfaces where they adsorb. Platinum particles in  
15 carbon supported ORR catalysts with high metal contents (20%) disrupt the self-assembly of  
16 Nafion® and virtually eliminate the oxygen confinement, but the phenomenon is still observed for  
17 low Pt loading (4.8%) catalysts.  
18  
19  
20  
21  
22  
23  
24  
25  
26  
27  
28  
29  
30  
31  
32  
33  
34  
35  
36  
37  
38  
39  
40  
41  
42  
43  
44  
45  
46  
47  
48  
49  
50  
51  
52  
53  
54  
55  
56  
57  
58  
59  
60

## INTRODUCTION

In a recent paper, we reported the existence of oxygen adsorption on the surface of a polyaniline-based heat-treated Fe/N/C catalyst of oxygen reduction reaction (ORR) in sulfuric acid media.<sup>1</sup> The adsorption isotherm exhibited the Langmuirian<sup>2</sup> characteristics, *i.e.*, did not display any noticeable repulsive or attractive interactions between oxygen molecules in the adsorbed layer. As the amount of adsorbed oxygen correlated with the surface density of the iron sites, we postulated that the adsorption occurred either in the close proximity of or directly on the catalytically active Fe sites. Based on previous work,<sup>3-5</sup> the latter comprise of iron centers coordinated by four in-plane pyridinic nitrogen atoms belonging to either a single (N<sub>4</sub>) or two separate (N<sub>2+2</sub> – coordination) graphene planes and arranged like in two phenanthroline molecules. In the course of our more recent studies<sup>6</sup> on oxygen reduction catalysis by transition metal macrocyclic complexes, *e.g.*, porphyrins, phthalocyanines and corroles, we found the presence of similar adsorption phenomena. The active centers of the macrocyclic complexes are structurally similar to those postulated for the Fe/N/C composites in that they have a similar in-plane N<sub>4</sub> coordination of the metal centers and a  $\pi$ -electron rich environment surrounding them. However, an interesting fact about the oxygen adsorption observed for the macrocycles was that it occurred irrespective of whether the active center was Fe (III) or Co(II). Intrigued by the above finding, we performed a detailed study of the phenomenon. We found that it was induced by self-assembly of Nafion® on carbon<sup>6</sup> in the catalyst inks. The results and conclusions of the study are presented in the following sections of the manuscript.

## EXPERIMENTAL

1  
2  
3 The following macrocyclic complexes were obtained from Aldrich and used as received:  
4  
5 Iron(III) tetraphenylporphyrin chloride (5,10,15,20-Tetraphenyl-21*H*,23*H*-porphine iron(III)  
6  
7 chloride, >94%, hereafter called FeTPPCL), iron(III) phthalocyanine chloride (~95%, hereafter  
8  
9 called FePCCl), iron(III) octaethylporphyrin chloride (2,3,7,8,12,13,17,18-octaethyl-21*H*,23*H*-  
10  
11 porphine iron(III) chloride, hereafter called FeOEPCl), cobalt(II) phthalocyanine (97%, hereafter  
12  
13 called CoPC), cobalt(II) tetramethoxyphenylporphyrin (5,10,15,20-tetrakis(4-methoxyphenyl)-  
14  
15 21*H*,23*H*-porphine cobalt(II), 97%, hereafter called CoTMeOPP), cobalt(II) octaethylporphyrin  
16  
17 (2,3,7,8,12,13,17,18-Octaethyl-21*H*,23*H*-porphine cobalt(II), hereafter called CoOEP), cobalt(II)  
18  
19 tetraphenylporphyrin (5,10,15,20-Tetraphenyl-21*H*,23*H*-porphine cobalt(II), 85%, hereafter  
20  
21 called CoTPP).  
22  
23  
24  
25

26  
27 Anhydrous dichloromethane (DCM,  $\geq 99.8\%$  with 50-150 ppm amylene as stabilizer, Sigma  
28  
29 Aldrich) and Vulcan XC72, a high surface area ( $205 - 250 \text{ m}^2 \text{ g}^{-1}$ )<sup>7-10</sup> carbon with the average  
30  
31 particle size between 30 nm and 40 nm<sup>11-12</sup>(Cabot) were used as received.  
32  
33

34 All experiments were performed using  $0.5 \text{ mol dm}^{-3} \text{ H}_2\text{SO}_4$  at 25 °C as the background  
35  
36 electrolyte. The electrolyte was prepared using a commercial sulfuric acid (Certified ACS Plus,  
37  
38 Fisher Chemical) and Millipore® water.  
39  
40

41 The working electrode in RRDE experiments was a Pine model AFE7R9GCPT electrode with  
42  
43 a glassy carbon disk and a platinum ring. Its nominal collection efficiency of 37% was confirmed  
44  
45 by independent measurements using potassium ferricyanide in potassium chloride electrolyte  
46  
47 solutions. In some voltammetric experiments a 3 mm glassy carbon disk (Bioanalytical Systems),  
48  
49 a 1.6 mm Pt disk (Bioanalytical Systems) and homemade 4.8 mm highly oriented pyrolytic  
50  
51 graphite (HOPG) disk electrodes were used. The latter were fabricated by masking a  
52  
53 7 mm x 7mm x 1 mm HOPG platelet from SPI Supplies (grade SPI-2, mosaic angle  $0.8^\circ \pm 0.2^\circ$ ,  
54  
55  
56  
57  
58  
59  
60

1  
2  
3 the lateral grain size up to 0.5 - 1 mm) with polyimide Kapton® tape using the methodology  
4 described previously.<sup>6</sup>  
5  
6

7  
8 The deposition of Pt nanoparticles on HOPG was performed using a technique similar to that  
9 applied by Ju and coworkers for palladium.<sup>13</sup> A freshly prepared HOPG disk electrode was placed  
10 under potential (0.84 V vs. RHE) in a 2 mM H<sub>2</sub>PtCl<sub>6</sub> solution in 0.5 M H<sub>2</sub>SO<sub>4</sub>. The potential was  
11 applied in order to prevent a spontaneous Pt deposition. After 10 seconds, a 100 ms potential pulse  
12 to 5 V was applied to create oxidized surface sites for Pt deposition. Ten seconds after the first  
13 pulse, a 20 ms potential pulse (-0.06 V vs. RHE) was applied to initiate fast H<sub>2</sub>PtCl<sub>6</sub> reduction  
14 guaranteeing instantaneous Pt nucleation. After the pulse, the potential was changed to 0.24 V vs.  
15 RHE in order to deposit Pt on the nuclei deposited at -0.06 V. The electrode was held at 0.24 V  
16 vs. RHE for 20 s after which the potential was changed again to 0.84 V to stop the growth of Pt  
17 particles. The electrode was removed under potential from the solution, rinsed with Millipore water  
18 and dried in air. The electrochemically active surface area of such deposited Pt (typically  
19 ~2.4 x 10<sup>-2</sup> cm<sup>2</sup>) was determined from cyclic voltammetry in deoxygenated sulfuric acid solution  
20 and corresponded to ~13% of the surface area of the HOPG disk. Neither the size nor the surface  
21 distribution of the particles was determined.  
22  
23  
24  
25  
26  
27  
28  
29  
30  
31  
32  
33  
34  
35  
36  
37  
38  
39  
40

41 The counter electrode in all experiments was a graphite rod, whereas the reference electrode was  
42 a hydrogen electrode utilizing 6% H<sub>2</sub> in Ar in equilibrium with Pt black coated platinum wire  
43 immersed in 0.5 mol dm<sup>-3</sup> H<sub>2</sub>SO<sub>4</sub>. The equilibrium potential of the reference electrode at Los  
44 Alamos elevation (2100 m above sea level) is 39 mV positive than the potential of a reversible  
45 hydrogen electrode (RHE) in the respective solution at the sea level.<sup>1</sup>  
46  
47  
48  
49  
50  
51  
52

53 Oxygen concentration in the studied solutions was adjusted by using either pure oxygen or its  
54 mixtures with argon as the purging gas. The actual oxygen concentration in solution was  
55  
56  
57  
58  
59  
60

1  
2  
3 determined from the corresponding limiting RRDE currents corrected for the number of electrons  
4 transferred in ORR and the respective corrected currents measured for oxygen saturated solution  
5  
6  
7  
8  
9 (8.65 x 10<sup>-4</sup> mol dm<sup>-3</sup> at Los Alamos elevation of 2100 m<sup>1</sup>).

10 Two well characterized<sup>7, 11, 14-16</sup> Pt catalysts supported on Vulcan were used in the study: 20%  
11 Pt (BASF) and 4.8% Pt (TEC10V05E, Tanaka Kikinzoku Kogyo). The third studied Pt (4.8%)  
12 catalyst was supported on graphitized carbon. Its properties were not disclosed by the  
13 manufacturer. The X-ray diffraction and BET measurements were performed by the authors of the  
14 paper. In similarity to Vulcan, the carbon support in that catalyst exhibited low porosity (<2 nm),  
15 but the BET surface area of the catalyst (157 m<sup>2</sup> g<sup>-1</sup>) was significantly lower than that of Vulcan,  
16 whereas the Pt particle size (4.8 nm from Scherrer equation<sup>17</sup>) larger than that (2.1 - 2.6 nm) for  
17 the remaining Pt catalysts.<sup>7, 14-16</sup> As in our previous paper,<sup>6</sup> the three Pt catalysts will be hereafter  
18 called Pt20V (20% BASF), Pt4.8V (4.8% Tanaka), and Pt4.8G (Pt on graphitized support),  
19 respectively.  
20  
21  
22  
23  
24  
25  
26  
27  
28  
29  
30  
31  
32  
33

34 The catalyst inks for macrocyclic ORR catalysts were prepared using the procedure described in  
35 our previous paper.<sup>6</sup> Briefly, ~40 mg of Vulcan XC72 were mixed with a few milligrams of the  
36 desired macrocycle and 2 - 4 cm<sup>3</sup> of dichloromethane and slowly sonicated to dryness. The residue  
37 was sonicated for around 1 hour with 8 cm<sup>3</sup> of isopropanol (IPA) and small quantities of 5%  
38 Nafion® solution (Ion Power, Inc.). The inks of Pt catalysts were prepared by mixing the solids  
39 with IPA and Nafion® followed by sonication. The amount of 5% Nafion® solution in the catalyst  
40 inks will be denoted<sup>6</sup> by R and corresponds to the ratio of volume of the 5% Nafion® solution  
41 expressed in microliters to the mass of the carbon support expressed in milligrams. The value of  
42 R varied from 0 to 2.7 µl per 1 mg of the carbon support, *i.e.*, R = 1 corresponds to 1 µl of the  
43  
44  
45  
46  
47  
48  
49  
50  
51  
52  
53  
54  
55  
56  
57  
58  
59  
60



1  
2  
3 Nafion® solution used for 1 mg of the carbon support and is equivalent to 46.8 µg of pure Nafion®  
4  
5 per 1 mg of the support. All inks were stored in tightly closed glass vials at room temperature.  
6  
7

8 A Pine Instruments bipotentiostat model AFCBP1 controlled by Aftermath software (Pine  
9 Instruments) was used in all experiments. Unless otherwise stated, all experiments were performed  
10 for a constant total loading of 0.1 mg of the carbon support, which corresponds to  
11  
12 ~0.4 mg<sub>carbon</sub> cm<sub>disk</sub><sup>-2</sup>. The deposition of the inks on the glassy carbon disk of the RRDE and its  
13  
14 evaporation were monitored under a microscope.  
15  
16  
17  
18  
19

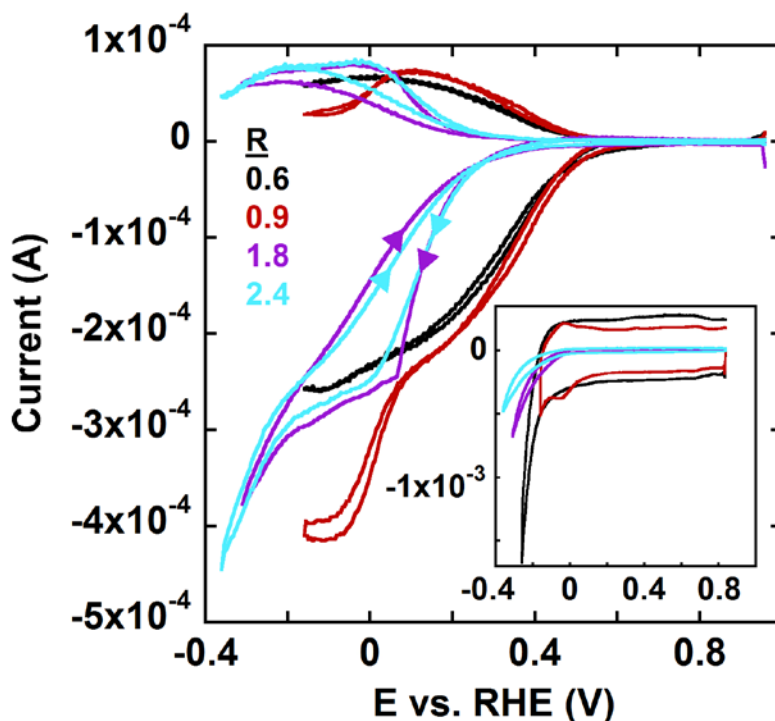
## 20 21 RESULTS

### 22 23 24 *1. Cyclic voltammetry of oxygen on Vulcan supported Co and Fe macrocycles*

25  
26  
27 As shown in our previous paper,<sup>6</sup> cobalt phthalocyanine exhibits most stable electrochemical  
28 behavior among the macrocycles selected for the present study. Therefore, it was selected to  
29 demonstrate the concepts and approaches applied to quantify the surface confinement of oxygen  
30 and major relationships governing the phenomenon.  
31  
32  
33  
34  
35  
36

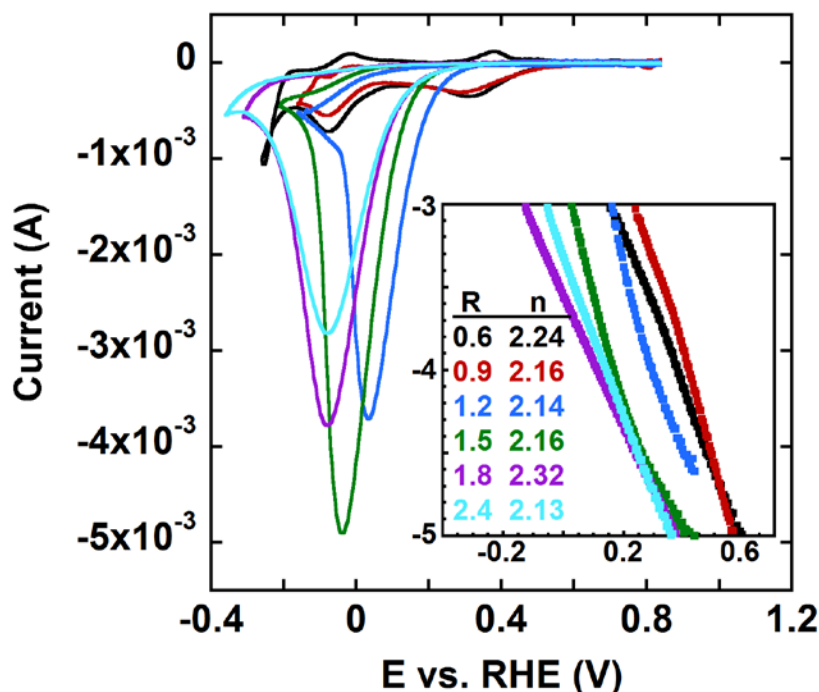
37 Figure 1 shows selected RRDE voltammograms for ORR catalyzed by carbon (Vulcan XC72)  
38 supported CoPC (5.7%). In agreement with our previous work,<sup>6</sup> higher Nafion® contents ( $R \geq 1.2$ ,  
39 for picture clarity the data for  $R = 1.2$  and  $R = 1.5$  not shown in Fig. 1) leads to significant ORR  
40 inhibition. The inhibition is associated with the blocking of the carbon surface by the hydrophobic  
41 component of Nafion,<sup>6</sup> as demonstrated by the significant suppression of the respective  
42 background currents (inset in Fig. 1). Within the studied potential range (up to -0.36 V vs. RHE),  
43 two oxygen reduction steps can be seen for  $R \leq 0.9$ , but the inhibition of the reaction obscures the  
44 second reduction step at  $R \geq 1.2$  (shown for  $R \geq 1.8$  in Fig. 1). A hysteresis is also observed  
45 between the forward and reverse scans of the voltammograms recorded for the inks, where the  
46  
47  
48  
49  
50  
51  
52  
53  
54  
55  
56  
57  
58  
59  
60

1  
2  
3 surface blocking takes place (Fig. 1). The hysteresis was found to decrease with the electrode  
4 rotation rate, which suggested that the currents in the forward scans were enhanced by oxygen  
5 rotation rate, which suggested that the currents in the forward scans were enhanced by oxygen  
6 adsorption, but no controlled study of the phenomenon was performed under RRDE conditions.  
7  
8  
9



37 Figure 1. Background corrected RRDE voltammograms of oxygen saturated 0.5 mol dm<sup>-3</sup> H<sub>2</sub>SO<sub>4</sub>  
38 solution recorded for a 5.7% CoPC on Vulcan XC72. Total carbon loading 0.1 mg. Rotation rate  
39 400 rpm. Scan rate 10 mV s<sup>-1</sup>. Nafion® contents (R) in the catalyst inks listed in the figure. Inset:  
40 cyclic voltammograms (100 mV s<sup>-1</sup>) recorded for the same catalysts in deoxygenated 0.5 mol dm<sup>-3</sup>  
41 H<sub>2</sub>SO<sub>4</sub> solutions.  
42  
43  
44  
45  
46  
47  
48  
49  
50  
51  
52  
53  
54  
55  
56  
57  
58  
59  
60

1  
2  
3 The surface (diffusionless) character of the current enhancement was confirmed by standard  
4 cyclic voltammetry without electrode rotation. The respective stationary voltammograms  
5 exhibited tall and rather symmetrical oxygen reduction peaks whose heights increased with the  
6 electrode equilibration time at the open circuit. Typical voltammograms demonstrating the  
7 presence of surface confined oxygen for  $R \geq 1.2$  are presented in Fig. 2.



38  
39  
40  
41 Figure 2. Cyclic voltammograms of oxygen saturated  $0.5 \text{ mol dm}^{-3} \text{ H}_2\text{SO}_4$  solution recorded for a  
42 5.7% CoPC on Vulcan XC72. Total carbon loading  $0.1 \text{ mg}$ . Scan rate  $500 \text{ mV s}^{-1}$ . Equilibration  
43 time 5 min at 400 rpm. Nafion® contents in the catalyst inks listed in the figure. Inset: kinetic  
44 ORR currents determined for the same catalysts from RRDE experiments at 400 rpm. Nafion®  
45 contents (R) in the catalyst inks and the respective numbers of electrons (n) transferred in ORR  
46 listed in the figure.

1  
2  
3 In agreement with the RRDE data (Fig. 1), two oxygen reduction peaks corresponding to the  
4 two ORR steps can be seen in the voltammograms recorded for  $R = 0.6$  and  $R = 0.9$  (Fig. 2). Two  
5 smaller reoxidation peaks are also seen in the reverse scans of these voltammograms. The ratios  
6 of the reverse to the forward peak currents were found to increase with scan rate and the reverse  
7 (anodic) peaks were almost absent at  $100 \text{ mV s}^{-1}$ . No mechanistic study of the reactions  
8 corresponding to the two red-ox systems was performed. However, the first CoPC reduction was  
9 found to correspond to around 100% generation of hydrogen peroxide (see inset in Fig. 2) under  
10 RRDE conditions, whereas the number of electrons involved in the ORR at the potentials of the  
11 second step (visible in the studied potential range only at  $R \leq 0.9$ ) was higher than 2, but did not  
12 exceed 3. Upon the increase in  $R$  from 0.9 to 1.2, the two red-ox systems disappeared and were  
13 replaced by a large and relatively symmetrical oxygen reduction peak. Its position, height and  
14 width depended on Nafion® concentration in the catalyst layer. The peak width increased with  $R$ ,  
15 whereas the peak current increased upon transition from  $R = 1.2$  to  $R = 1.5$ , but then decreased  
16 with further  $R$  increase (Fig. 2). The peak position correlated with the ORR kinetics determined  
17 from the reverse scans of respective RRDE voltammograms (inset in Fig. 2).  
18  
19  
20  
21  
22  
23  
24  
25  
26  
27  
28  
29  
30  
31  
32  
33  
34  
35  
36  
37

38 The voltammograms in Fig. 2 were recorded after 5 minute electrode equilibration (with 400 rpm  
39 rotation) at the open circuit potential in fully oxygenated solution. When applicable ( $R \geq 1.2$ ), such  
40 conditions guaranteed equilibrium between the fully oxygenated solution and the surface confined  
41 oxygen as determined from a series of voltammetric experiments performed after different  
42 equilibration times. An identical procedure was used to determine the equilibration times required  
43 to reach the surface confinement equilibrium for all other catalysts and oxygen concentrations in  
44 this study.  
45  
46  
47  
48  
49  
50  
51  
52  
53  
54  
55  
56  
57  
58  
59  
60

1  
2  
3 While the symmetry and the height of the voltammetric peaks measured for  $R \geq 1.2$  (Fig. 2)  
4 leaves no doubt that the major contribution to the measured currents originates from the reaction  
5 of surface confined oxygen, the measured currents are influenced by contributions from oxygen  
6 diffusing from the bulk of solution and the number of electrons involved in the reaction (inset in  
7 Fig. 2). Similarly, the peak widths and positions depend on the actual charge transfer kinetics (inset  
8 in Fig. 2). Such factors together with the adsorption kinetics have to be taken into account in order  
9 to correctly determine the equilibrium concentration of surface confined oxygen.  
10  
11  
12  
13  
14  
15  
16  
17  
18  
19

20 The reduction charge of surface confined oxygen can be determined using a relatively simple  
21 procedure whose principle is briefly described below. If the geometric surface density of the ORR  
22 active sites is sufficient to result in planar diffusion of oxygen towards the electrode and there is  
23 no significant interplay between the completely irreversible reduction of surface confined oxygen  
24 and that diffusing from the bulk of solution, the peak currents ( $i_p$ ) corresponding to the two  
25 completely irreversible reaction mechanisms should be described by the equations derived by  
26 Laviron<sup>18</sup> and Nicholson and Shain,<sup>19</sup> respectively. These equations predict linear dependencies of  
27 the peak current on either the scan rate ( $v$ )<sup>18</sup> or its square root ( $v^{1/2}$ ).<sup>19</sup> One can also demonstrate  
28 that similar current( $i$ ) *vs.*  $v$  and current *vs.*  $v^{1/2}$  relationships should hold for the respective processes  
29 at any fixed difference ( $\Delta E$ ) between the measured potential ( $E$ ) and the respective peak potential  
30 ( $E_p$ ):  
31  
32  
33  
34  
35  
36  
37  
38  
39  
40  
41  
42  
43  
44  
45

$$i_{\Delta E \text{ surface}} = B_{\Delta E \text{ surface}} \cdot v \quad (1)$$

$$i_{\Delta E \text{ solution}} = B_{\Delta E \text{ solution}} \cdot v^{1/2} \quad (2)$$

46 where  $i_{\Delta E \text{ surface}}$  and  $i_{\Delta E \text{ solution}}$  represent the currents of the surface confined and the dissolved  
47 species, whereas the constants  $B$  are different for the diffusing and surface confined species and  
48 depend on the selected  $\Delta E$  for each process. The integration of eqs. 1 and 2 against time over  $\Delta E$   
49 results in:  
50  
51  
52  
53  
54  
55  
56  
57  
58  
59  
60

$$\int_{\Delta E} i_{surface} = G(\Delta E_{surface}) \quad (3)$$

$$\int_{\Delta E} i_{solution} = H(\Delta E_{solution}) \cdot v^{-1/2} \quad (4)$$

where G and H are  $\Delta E$  – dependent constants. If a sufficiently wide range of  $\Delta E$  on both sides of the surface reduction peak is selected, the integral in eq. 3 becomes equal to the charge corresponding to the complete reduction of the surface confined species.

$$G(\Delta E \rightarrow \infty) \rightarrow Q_{surface} \quad (5)$$

The integration of an experimental voltammetric current containing the contributions from both adsorbed and dissolved species over a specific potential range fixes the  $\Delta E_{solution}$  and  $\Delta E_{surface}$  potential ranges. When the scan rate is changed, both of these ranges ( $\Delta E_{solution}$  and  $\Delta E_{surface}$  as measured vs. the respective peak potentials) cannot be preserved simultaneously by adjusting the overall potential range  $\Delta E$  because of the generally different  $E_p$  vs.  $v$  relationships for surface confined<sup>18</sup> and dissolved<sup>19</sup> species. Consequently, the scan rate dependence of the electrolysis charge in a specific potential range  $\Delta E$  measured vs. the peak potential cannot be expressed as an exact sum of eqs. 3 and 4 with scan rate independent parameters G and H. However, if the potential range for the integration is significantly wider than the expected differences in the scan rate induced shifts of the peak potentials for the confined and dissolved species, an approximate relationship should still hold:

$$Q \approx Q_{surface} + H \cdot v^{-1/2} \quad (6)$$

The accuracy of eq. 6 is expected to improve with scan rate, which reduces the second term in the equation corresponding to the contribution from the dissolved species. The equation provides means to determine the reduction charge of the surface confined oxygen ( $Q_{\text{surface}}$ ). The charges of interest can be extracted from the intercepts of the respective  $Q$  vs.  $v^{-1/2}$  plots. The procedure was successfully used by us previously to determine the amount of surface confined oxygen for a pyrolyzed Fe/N/C catalyst.<sup>1</sup>

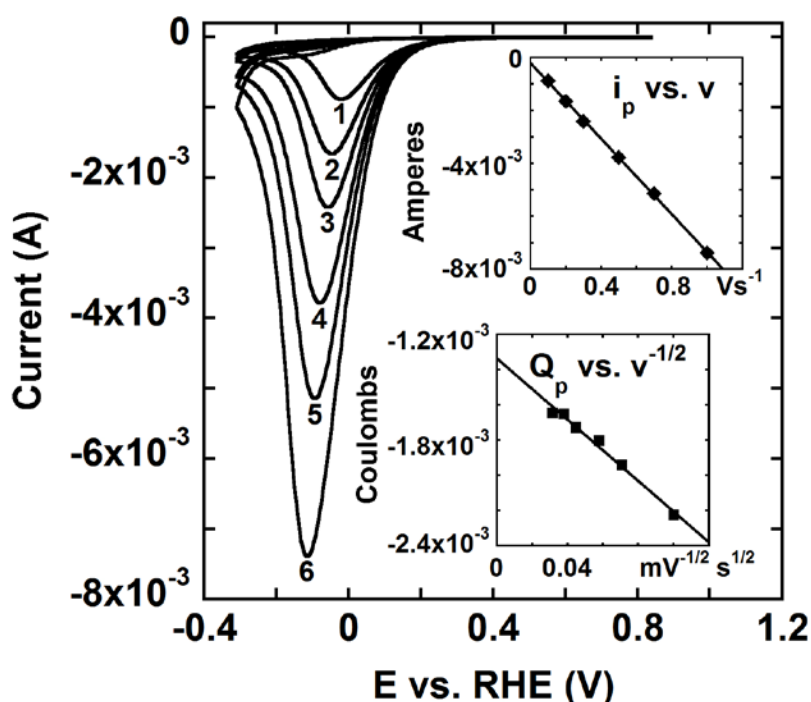


Figure 3. Cyclic voltammograms of oxygen saturated 0.5 mol dm<sup>-3</sup> H<sub>2</sub>SO<sub>4</sub> solution recorded for 5.7% CoPC on Vulcan XC72. Total carbon loading 0.1 mg. Equilibration time 5 min at 400 rpm.  $R = 1.8$ . Scan rate (mV s<sup>-1</sup>): 100 (1), 200 (2), 300 (3), 500 (4), 700 (5), 1000 (6). Top inset: peak current vs. scan rate. Bottom inset: oxygen reduction charge plotted vs. inverse square root of the scan rate (see text for the charge determination methodology).

1  
2  
3 In Fig. 3 are shown the voltammograms recorded for the 5.7% CoPC catalyst at different scan  
4 rates after 5 minute equilibration at 400 rpm in fully oxygenated solution. As demonstrated by the  
5 virtually linear dependence between the peak current and the square root of the scan rate (top  
6 inset), the contribution of oxygen diffusing from the bulk to the measured currents is small.  
7  
8 Consequently, eq. 5 quite accurately describes the measured reduction charge  $Q$  and the respective  
9  
10  $Q_{\text{surface}}$  can be reliably determined from a linear extrapolation of the measured charge  $Q$  against  
11  
12 the inverse square root of time to zero. The corresponding linear relationship between  $Q$  and  $v^{-1/2}$   
13  
14 is presented in the bottom inset in Fig. 3.  
15  
16  
17  
18  
19  
20  
21

22 The voltammetry of oxygen in presence of other macrocycles in this study and at lower than  
23 saturated oxygen concentrations was qualitatively similar to that described above for CoPC in  
24 presence of oxygen saturated solutions (Figs. 1 – 3). The respective ORR peaks were  
25 predominantly transport controlled for low Nafion® contents in the catalyst layers and exhibited  
26 mostly diffusionless character at higher Nafion® contents, which promoted self-assembly of  
27 Nafion®. The results obtained for the iron macrocycles, especially FePCCl and FeTPPCL, were  
28 affected by the low complex durability under the ORR conditions and were excluded from  
29 quantitative analysis.  
30  
31  
32  
33  
34  
35  
36  
37  
38  
39

40 For the vast majority of catalyst layer compositions, including different macrocycles and  
41 Nafion® contents, the kinetics of the processes leading to oxygen confinement was fast enough to  
42 guarantee the equilibrium surface concentration of oxygen in less than five minutes at 400 rpm.  
43  
44 As no detailed kinetic studies were performed, no strictly quantitative conclusions regarding  
45 structural and catalyst concentration effects on the kinetics of the phenomenon could be reached.  
46  
47 However, two observations were made. First, the kinetics of oxygen adsorption was faster for all  
48 studied systems than that observed by us previously for the previously mentioned.  
49  
50  
51  
52  
53  
54  
55  
56  
57  
58  
59  
60



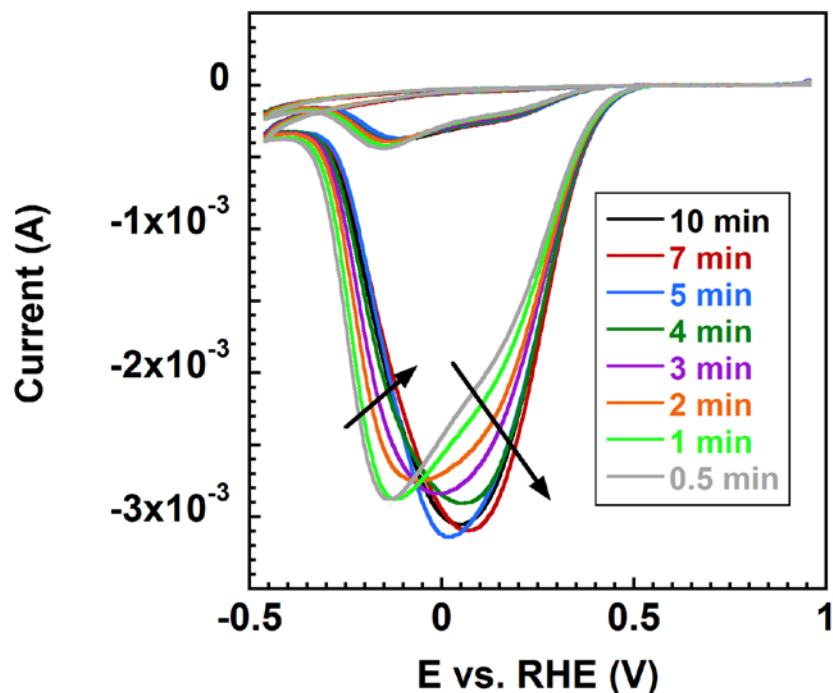


Figure 4. Two cycle voltammograms of oxygen saturated  $0.5 \text{ mol dm}^{-3} \text{ H}_2\text{SO}_4$  solution recorded for 8.1% CoTPP on Vulcan XC72 after different equilibration times at 400 rpm. Total carbon loading 0.1 mg.  $R = 1.6$ . Scan rate  $1000 \text{ mV s}^{-1}$ .

pyrolyzed Fe/polyaniline catalyst.<sup>1</sup> Second, the peak potentials and widths for oxygen reduction correlated quite well with the kinetic ORR parameters determined for dissolved oxygen from the reverse (anodic) RRDE scans. However, the correlations were also influenced by the equilibration time, which moderately affected the shape and position of the reduction peaks. The phenomenon is illustrated in Fig. 4 for 8.1% CoTPP catalyst ( $R = 1.6$ ), where the observed changes were most prominent. They demonstrate an improvement in ORR catalysis of surface confined oxygen with the equilibration time. The enhancement of the apparent kinetics of the reduction of surface confined oxygen can hardly be attributed to changes in the intrinsic catalytic activity of the active sites. It most likely reflects potential-induced morphological changes in the catalyst layer, which affect the accessibility of the active sites and thus the apparent ORR kinetics.<sup>6</sup> The changes in

1  
2  
3 morphology most likely involve Nafion®<sup>20</sup> and the catalytically active molecules or their mobile  
4 fragments, *e.g.*, side phenyl groups in CoTPP. The changes did not measurably affect the reduction  
5 charges of oxygen corresponding to adsorption equilibrium.  
6  
7  
8  
9

## 10 11 **2. Oxygen adsorption on macrocycle covered Vulcan XC72**

12  
13  
14 The equilibrium surface concentrations of oxygen for all studied catalyst compositions were  
15 determined using the procedure demonstrated for 5.7% CoPC to measure charges of the adsorbed  
16 oxygen (Fig. 3). The latter were subsequently corrected for the number of electrons involved in  
17 ORR to determine the number of moles of the adsorbed oxygen. In order to get accurate results,  
18 the number of electrons was determined from the respective forward (cathodic) RRDE scans,  
19 where surface confined oxygen contributed to the measured currents (Fig. 1). Moreover, the same  
20 electrode equilibration times were used in both voltammetric and RRDE experiments and the  
21 number of electrons from RRDE experiments was averaged over the potential range used for the  
22 charge integration in voltammetry. The effects of various factors on oxygen adsorption were  
23 studied and included the amount of Nafion® in the catalyst layer, the catalyst loading and  
24 composition, and the concentration of oxygen in solution.  
25  
26  
27  
28  
29  
30  
31  
32  
33  
34  
35  
36  
37  
38  
39  
40

### 41 **2.1. Nafion® content and active site concentration effects on oxygen confinement on Vulcan** 42 **supported catalysts**

43  
44  
45 The effect of Nafion® quantity in the catalyst layer was studied for four catalysts containing  
46 CoPC as the active molecule and using exclusively oxygen saturated solutions. For three catalysts  
47 (1.7%, 5.7%, 13.6% CoPC), desired quantities of Nafion® were directly added to the catalyst inks,  
48 which were subsequently deposited on the RRDE tip. The fourth catalyst (5.4% CoPC) was  
49 deposited onto the electrode using an ink containing no Nafion®. Subsequently, a small quantity  
50  
51  
52  
53  
54  
55  
56  
57  
58  
59  
60

1  
2  
3 of the solution obtained by 100-fold dilution with water of the commercial 5% Nafion® was  
4 deposited on top of the dry catalyst layer to obtain the desired Nafion® content in the layer. The  
5 surface concentrations of oxygen were determined using the procedure described in the previous  
6 section and assuming that the whole Vulcan XC72 surface area ( $\sim 240 \text{ m}^2 \text{ g}^{-1}$ ) participated in the  
7 oxygen confinement. The surface concentrations of oxygen are plotted in Fig. 5 together with the  
8 respective background currents measured at 0.3 V vs. RHE and  $100 \text{ mV s}^{-1}$ . The data in Fig. 5  
9 demonstrate a correlation between the surface confinement of oxygen ( $\Gamma_{\text{O}_2}$ ) and the suppression  
10 of the background currents by Nafion®. As the latter results from self-assembly of Nafion® on  
11 the carbon surface in the Nafion® containing inks,<sup>6</sup> the observed changes in  $\Gamma_{\text{O}_2}$  and background  
12 currents have virtually stepwise character and the surface concentration of oxygen tends to  
13 stabilize around  $2.4 \times 10^{-11} \text{ mol cm}^{-2}$  at high R, irrespective of the CoPC content in the catalyst. As  
14 demonstrated in our previous paper,<sup>6</sup> the actual number of active CoPC sites in the CoPC catalysts  
15 was not proportional to the mass percentage of CoPC due to carbon/CoPC agglomeration  
16 phenomena. However, the number of active sites per mass of the carbon support for the 13.6%  
17 CoPC catalyst can be estimated from the background currents and the measured ORR activities as  
18 up to 3 times higher than that for the catalysts with 1.7% and 5.7% CoPC. Consequently, a  
19 threefold increase in the number of active CoPC sites has virtually no effect on the observed  
20 surface confinement of oxygen.  
21  
22  
23  
24  
25  
26  
27  
28  
29  
30  
31  
32  
33  
34  
35  
36  
37  
38  
39  
40  
41  
42  
43  
44  
45  
46  
47  
48  
49  
50  
51  
52  
53  
54  
55  
56  
57  
58  
59  
60

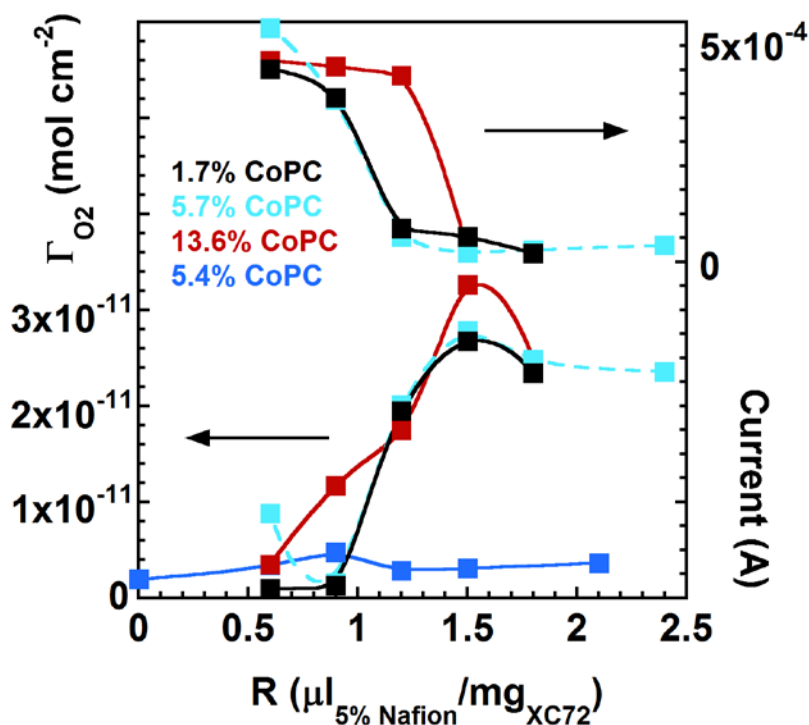


Figure 5. Oxygen surface concentrations (bottom) and voltammetric background currents measured at 0.3 V vs. RHE and 100 mV s<sup>-1</sup> (top) plotted against Nafion® content (R) in the catalyst layer. The background currents are sums of absolute currents measured in negative and positive scans. For the 5.4% CoPC catalyst, Nafion® was deposited on top of the Nafion® free catalyst layer as an aqueous solution obtained by 100-fold dilution of the commercial 5% solution.

## 2.2. Oxygen adsorption isotherms for Vulcan supported macrocyclic complexes and their mixtures with respective ligands

Oxygen adsorption isotherms were determined for selected macrocyclic complexes and mixtures of the complexes with their respective ligands at selected Nafion® contents (R) guaranteeing the maximum carbon surface blockage by Nafion®.<sup>6</sup> The surface concentrations of oxygen were measured for four different oxygen concentrations in solution using the procedure outlined above.

1  
2  
3 Irrespective of the catalyst layer composition, a linear relationship was found between the surface  
4  
5 ( $\Gamma$ ) and bulk oxygen concentration. Such a relationship is described by the Henry's adsorption  
6  
7 isotherm, a limiting form of the Langmuir isotherm for low surface concentrations, where the  
8  
9 adsorbed molecules virtually do not interact with each other. A typical adsorption isotherm is  
10  
11 presented in Fig. 6, whereas the numerical data obtained for all macrocyclic catalysts are collected  
12  
13 in Table 1. Inspection of the data in Table 1 reveals the lack of major effects of the macrocyclic  
14  
15 complexes and their ligands on the surface confinement of oxygen. The non-specific character of  
16  
17 the confinement indicates that neither the complexes nor their bare ligands play an important role  
18  
19 in the phenomenon. On the other hand, the correlation between the surface confinement of oxygen  
20  
21 and the self-assembly of Nafion® implies that the latter is exclusively responsible for the  
22  
23 accumulation of oxygen on the surface. The only role played by the active centers in the  
24  
25 voltammetry of surface confined oxygen is its reduction. In order to confirm the correctness of the  
26  
27 above hypothesis, a series of experiments were performed with three carbon supported Pt catalysts.  
28  
29 Two of them (Pt4.8V - 4.8% Pt on Vulcan and Pt4.8G - 4.8% on graphitized carbon) were  
30  
31 previously demonstrated to promote self-assembly of Nafion®,<sup>6</sup> whereas the third one (Pt20V  
32  
33 - 20% Pt on Vulcan) did not support Nafion® adsorption up to and including  $R = 2.7$ . The results  
34  
35 obtained for the Pt catalysts are summarized in the following section.  
36  
37  
38  
39  
40  
41  
42  
43  
44  
45  
46  
47  
48  
49  
50  
51  
52  
53  
54  
55  
56  
57  
58  
59  
60

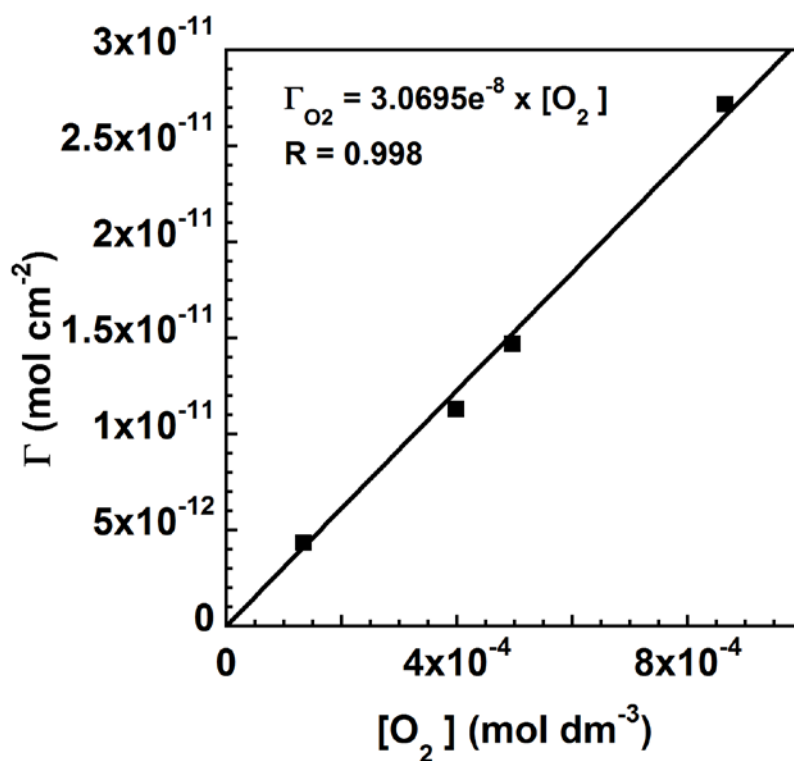


Figure 6. Oxygen adsorption isotherm for 8.1% CoTPP catalyst ( $R = 1.6$ ) in  $0.5 \text{ mol dm}^{-3} \text{ H}_2\text{SO}_4$  solution.

**Table 1. Equilibrium (Henry's) constants and concentrations of surface confined oxygen measured for Co and Fe macrocyclic complexes adsorbed on Vulcan XC72 in presence of self-assembled Nafion® layers.<sup>a)</sup>**

Catalyst	R ( $\mu\text{l}$ (5% Nafion)/ mg (XC72))	Henry's constant (cm)	Correlation coefficient	$\Gamma_{\text{meas}}^{\text{b)}$ (mol cm <sup>-2</sup> )	$\Gamma_{\text{calc}}^{\text{c)}$ (mol cm <sup>-2</sup> )
6.4% CoPC	1.3	$(2.63 \pm 0.04) \times 10^{-8}$	0.998	$2.22 \times 10^{-11}$	$2.28 \times 10^{-11}$
5.0% CoPC + 5.0% PC	1.3	$(2.36 \pm 0.55) \times 10^{-8}$	0.732	$2.10 \times 10^{-11}$	$2.04 \times 10^{-11}$
6.9% CoOEP + 6.5% OEP	1.5	$(3.20 \pm 0.08) \times 10^{-8}$	0.998	$2.83 \times 10^{-11}$	$2.77 \times 10^{-11}$
8.1% CoTPP	1.6	$(3.07 \pm 0.06) \times 10^{-8}$	0.998	$2.72 \times 10^{-11}$	$2.66 \times 10^{-11}$
6.0% CoTPP + 6.2% TPP	1.4	$(3.01 \pm 0.12) \times 10^{-8}$	0.991	$2.56 \times 10^{-11}$	$2.61 \times 10^{-11}$
9.8% FeOEPCI	1.7	$(2.56 \pm 0.26) \times 10^{-8}$	0.960	$2.53 \times 10^{-11}$	$2.22 \times 10^{-11}$

<sup>a)</sup>surface concentrations calculated assuming that the entire carbon surface participates in the surface confinement of oxygen

<sup>b)</sup>measured in O<sub>2</sub> saturated solution ( $8.65 \times 10^{-4}$  mol dm<sup>-3</sup>) at 2100 m above sea level

<sup>c)</sup>calculated from the adsorption isotherm for O<sub>2</sub> saturated solution ( $8.65 \times 10^{-4}$  mol dm<sup>-3</sup>) at 2100 m above sea level

### 3. Oxygen confinement in carbon supported Pt catalysts.

Figure 7 shows background corrected voltammograms ( $100 \text{ mV s}^{-1}$ ) of oxygen reduction on three Pt catalysts after 5 minute equilibration in oxygen saturated solutions. Only a slight distortion of the diffusion controlled ORR peak is observed for Pt20V with high Nafion® content ( $R = 1.8$ ), whereas the voltammograms recorded for the two low Pt content catalysts exhibit significantly

higher peaks whose shapes reveal their predominantly surface controlled character. There are also differences between the voltammograms recorded for these two catalysts. The voltammogram obtained for Pt4.8G exhibits higher currents in the whole cathodic

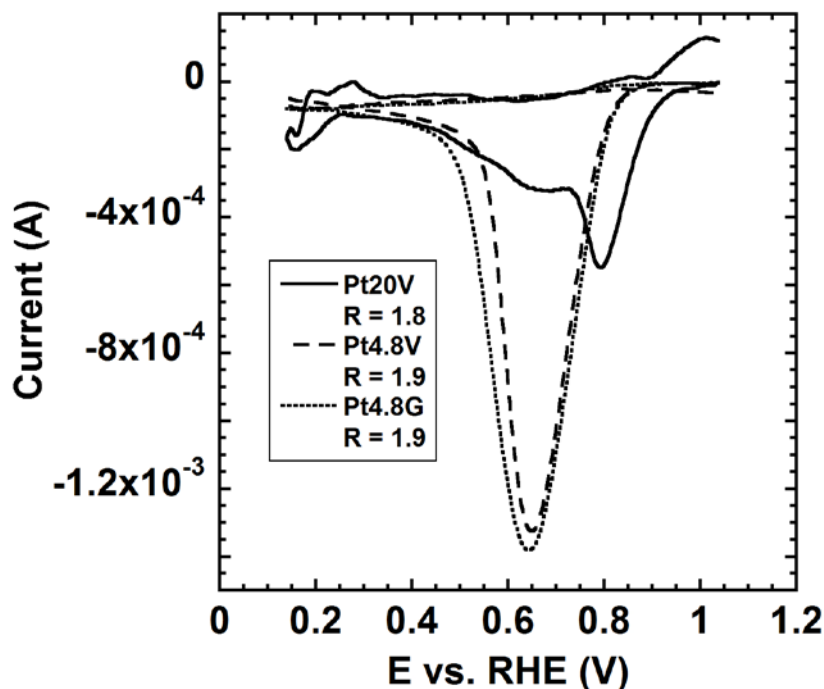


Figure 7. Background corrected cyclic voltammograms of oxygen saturated 0.5 mol dm<sup>-3</sup> H<sub>2</sub>SO<sub>4</sub> solution recorded for three Pt catalysts after 5 min equilibration at 400 rpm. Scan rate 100 mV s<sup>-1</sup>. Nafion® contents in the catalyst layers listed in the legend.

potential range than that recorded for its counterpart with non-graphitized support (Vulcan). The actual quantities of surface confined oxygen for the three Pt catalysts and different Nafion® contents were obtained from respective oxygen reduction charge vs.  $v^{-1/2}$  plots corrected by the number of electrons transferred in ORR. They are compared with the data obtained for the macrocyclic catalysts in Fig. 8. The quantities of surface confined oxygen in Figure 8 are referred to the mass of the carbon support rather than to its surface area, because the metal particles in the



different Pt catalysts occupy different and not exactly known fractions of the support surface areas and are affected (Pt4.8V and Pt 4.8G) or not (Pt20V)<sup>6</sup> by Nafion® self-assembly. Moreover, the surface properties of carbon supports do affect the distribution of Pt particles in supported catalysts,<sup>21-22</sup> which may influence Nafion® self-assembly in a similar way to that observed for Pt20V.

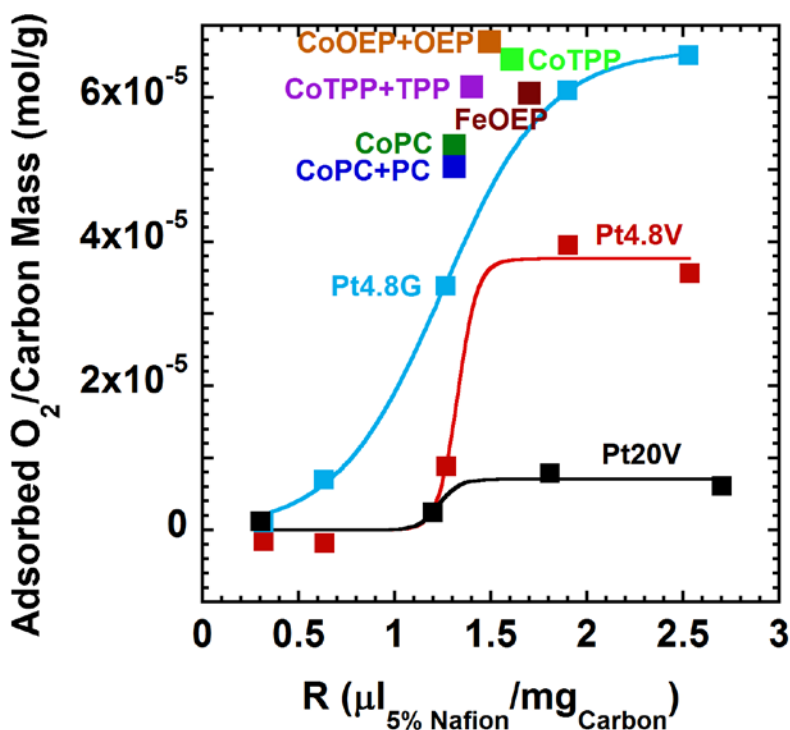


Figure 8. Molar concentrations of surface confined oxygen per gram of catalyst support in oxygen saturated  $0.5 \text{ mol dm}^{-3} \text{ H}_2\text{SO}_4$  solution plotted against Nafion® content in the catalyst layer for three Pt catalysts on different carbon supports and six macrocyclic complexes of Co and iron supported on Vulcan XC72. Macrocyclic catalyst compositions: CoPC (6.4%), CoPC + PC (5.0% CoPC, 5.0% PC), FeOEP (9.8% FeOEP/Cl), CoTPP (8.1%), CoTPP + TPP (6.0% CoTPP, 6.2% TPP), CoOEP + OEP (6.9% CoOEP, 6.5% OEP).

1  
2  
3 Figure 8 reveals that almost two times higher quantity of oxygen can be confined at the interfaces  
4 between the graphitized carbon and Nafion® (Pt4.8G) than between Vulcan and Nafion® (Pt4.8V)  
5 even though the specific surface area of Vulcan ( $205 - 250 \text{ m}^2 \text{ g}^{-1}$ )<sup>7-10</sup> is significantly higher than  
6 that of Pt4.8G ( $157 \text{ m}^2 \text{ g}^{-1}$ ). A comparable amount of oxygen per mass of the carbon support to  
7 that measured for Pt4.8G can be confined at the Vulcan/Nafion® interface for the studied  
8 macrocyclic catalysts. On the other hand, almost no oxygen can be confined at the Vulcan/Nafion®  
9 interface in Pt20V catalyst.  
10  
11  
12  
13  
14  
15  
16  
17  
18  
19

#### 20 21 **4. ORR catalyzed by Nafion® coated CoPC/HOPG and Pt/HOPG** 22 23

24 The data presented in the previous sections indicate that oxygen accumulates in the hydrophobic  
25 component of Nafion® self-assembled<sup>6</sup> on hydrophobic graphitic surfaces. Highly ordered  
26 pyrolytic graphite (HOPG) with its almost atomically flat graphitic surface and demonstrated  
27 ability to promote self-assembly of Nafion®<sup>6,23</sup> seemed to offer a unique opportunity to determine  
28 the quantitative relationship between the concentration of surface confined oxygen and the real  
29 graphitic surface area from ORR measurements. The expected contributions from surface  
30 confined oxygen in total oxygen reduction currents (charges) are much smaller for HOPG than  
31 those observed for the high surface area carbons. If 100% of the Vulcan surface area contributed  
32 to the oxygen confinement demonstrated in the previous sections, one could expect the geometric  
33 surface area charge density resulting from the reduction of oxygen confined on the surface of  
34 HOPG to be only around  $10 \mu\text{C cm}^{-2}$ . However, as proven by the results obtained for Pt4.8G, only  
35 a fraction of Vulcan surface area contributes to oxygen confinement, which gave us hope that the  
36 quantity of oxygen confined at HOPG/Nafion® interfaces would be sufficiently higher than  
37  $10 \mu\text{C cm}^{-2}$  to be accurately measurable.  
38  
39  
40  
41  
42  
43  
44  
45  
46  
47  
48  
49  
50  
51  
52  
53  
54  
55  
56  
57  
58  
59  
60

HOPG electrodes containing CoPC and Pt as oxygen reduction catalysts were prepared. The procedure to deposit Pt nanoparticles on HOPG is described in the experimental section. The method used to deposit CoPC on the graphite was as follows. A green and stable colloidal CoPC solution of known concentration in DCM was diluted with pure DCM to obtain a virtually colorless  $\sim 3.6 \times 10^{-5} \text{ mol dm}^{-3}$  CoPC suspension (or solution?) in DCM, which was subsequently deposited onto an HOPG disk and allowed to dry to produce a catalyst layer containing  $\sim 2 \times 10^{-9} \text{ mol cm}^{-2}$  CoPC (nominally in excess of 200 monolayers<sup>24</sup>) on the HOPG surface. As opposed to alcoholic (IPA and methanol) solutions of the other studied macrocycles, DCM was

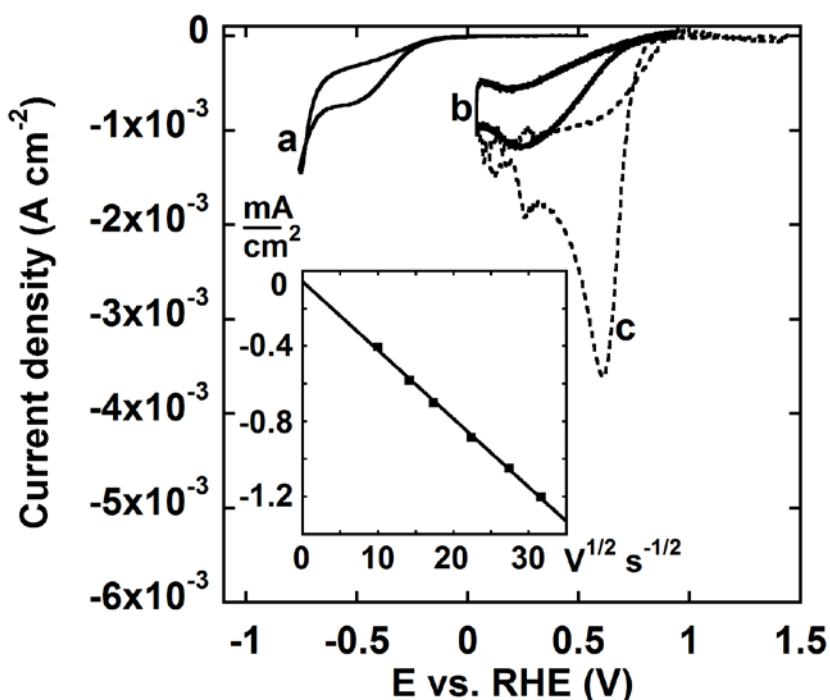


Figure 9. Background corrected cyclic voltammograms of oxygen saturated  $0.5 \text{ mol dm}^{-3} \text{ H}_2\text{SO}_4$  solution recorded for  $2 \times 10^{-9} \text{ mol cm}^{-2}$  CoPC (a) and Pt nanoparticles ( $0.024 \text{ cm}^2$  surface area, b) deposited on  $\sim 4.8 \text{ mm}$  HOPG disk and covered with a self-assembled Nafion<sup>®</sup> film as well as for an uncoated  $1.6 \text{ mm}$  Pt disk. Scan rate  $1 \text{ V s}^{-1}$ . Inset: peak current density for the HOPG/Pt/Nafion<sup>®</sup> electrode plotted against the square root of scan rate.

1  
2  
3 not causing Kapton delamination from HOPG. The CoPC catalyst layers fabricated in the above  
4  
5 way were found to lose almost 100% of their initial catalytic activity during a single voltammetric  
6  
7 scan in oxygenated H<sub>2</sub>SO<sub>4</sub> solutions. Their stability was significantly improved after the deposition  
8  
9 of thin Nafion® films, but even then it was impossible to measure both the background and the  
10  
11 ORR currents at more than a single scan rate without a visible loss in the electrode activity.  
12  
13 Consequently, we abandoned any quantitative comparison between uncoated and Nafion® coated  
14  
15 electrodes.  
16  
17  
18

19  
20 In Figure 9 are shown background corrected voltammograms (first scans) of oxygen recorded at  
21  
22 1 V/s for HOPG supported CoPC and Pt, coated with thin Nafion® films after 5 minute (CoPC)  
23  
24 or 10 minute (Pt) equilibration at their open circuit potentials in fully oxygenated H<sub>2</sub>SO<sub>4</sub> solution.  
25  
26 Such equilibration times deemed sufficient to guarantee an equilibrium between the dissolved and  
27  
28 surface confined oxygen. For comparison, a voltammogram measured under the identical  
29  
30 conditions using an uncoated 1.6 mm Pt disk (0.02 cm<sup>2</sup>) is also shown in Fig. 9.  
31  
32  
33

34  
35 As seen in Fig. 9, the peak current densities for both HOPG supported catalysts are significantly  
36  
37 lower than that measured for solid Pt. While the effect could be in part accounted for by the lower  
38  
39 ORR Tafel slopes measured for the HOPG supported catalysts, it is believed to predominantly  
40  
41 result from the spatial isolation of numerous active centers. When the distances between the active  
42  
43 centers (particles) are larger than the diameters of the respective diffusion layers around them, the  
44  
45 centers act as individual ultramicro- (or rather nano-) electrodes. The ORR current for such centers,  
46  
47 while enhanced by the hemispherical oxygen diffusion, will be lower than expected from the total  
48  
49 geometrical surface area they occupy and will exhibit a steady state character. The shape of  
50  
51 voltammograms in Fig. 9 suggests a significantly non-uniform active site distribution on the  
52  
53 HOPG surface. In some areas, the active centers are close enough to form a “uniformly” active  
54  
55  
56  
57  
58  
59  
60

1  
2  
3 surface. Such areas are responsible for planar oxygen diffusion towards the electrode and the  
4  
5 presence of the oxygen reduction peak current proportional to the square root of the scan rate (inset  
6  
7 in Fig. 9). In other areas, where the active particles are far apart, a hemispherical diffusion to the  
8  
9 individual sites occurs and contributes to the lower and time (scan rate) independent ORR currents  
10  
11 (non-zero intercept of the peak current vs. square root of the scan rate in the inset in Fig. 9). One  
12  
13 can imagine that oxygen potentially confined at the HOPG/Nafion® interface in the areas  
14  
15 surrounding the isolated Pt particles can no longer be reduced without a (surface) diffusion step.  
16  
17 Therefore, the separation of the reduction charges corresponding to the surface confined and bulk  
18  
19 oxygen, which was implemented in Eq. 6 can no longer be used to determine the quantity of surface  
20  
21 confined oxygen from the experimental results shown in Fig. 9. The determination of conditions  
22  
23 necessary to achieve a uniform and sufficiently dense distribution of platinum particles on HOPG,  
24  
25 which would enable the accurate determination of oxygen quantity trapped in the hydrophobic  
26  
27 Nafion® component at its interface with HOPG is the subject of a forthcoming study.  
28  
29  
30  
31  
32  
33

## 34 35 DISCUSSION AND CONCLUSIONS

36  
37  
38 The results obtained for the two Pt catalysts with low metal content show that the amount of  
39  
40 surface confined oxygen in presence of self-assembled Nafion® increases with the degree of  
41  
42 surface graphitization. As opposed to strongly hydrophobic graphitic surfaces,<sup>25-26</sup> amorphous  
43  
44 carbon surfaces lack highly delocalized  $\pi$  electrons responsible for surface hydrophobicity. The  
45  
46 atoms with unpaired electrons on amorphous surfaces easily undergo oxidation, which makes the  
47  
48 surface even less hydrophobic due to the presence of oxidized functional groups.<sup>27</sup> Such surfaces  
49  
50 are not expected to promote self-assembly of Nafion® through its hydrophobic component, as  
51  
52 observed previously<sup>6</sup> and in the present study. To the contrary, if the surface is sufficiently  
53  
54 hydrophilic, self-assembly of Nafion® through its hydrophilic component may occur.<sup>28</sup>  
55  
56  
57  
58  
59  
60

1  
2  
3 Consequently, graphitized carbon surfaces attract the hydrophobic Nafion® component much  
4 stronger than amorphous surfaces and are most likely exclusively responsible for the self-assembly  
5 of Nafion® and the resulting surface confinement of oxygen.  
6  
7  
8  
9

10 The responsibility of hydrophobic interactions between graphitic carbon surfaces and the  
11 hydrophobic Nafion® component for the self-assembly of Nafion® on the carbon supported  
12 catalysts and the resulting surface confinement of oxygen is intuitively understood. However, the  
13 potential role of other factors in both phenomena should not be underestimated. It cannot be  
14 assumed that the entire graphitic surface of a highly dispersed carbonaceous material actively  
15 participates in these phenomena. As demonstrated above, the presence of hydrophilic Pt particles  
16 in Pt catalysts lowers the extent of Nafion® self-assembly and the oxygen confinement. The  
17 magnitude of the effect is expected to depend on the distribution of the catalyst particles between  
18 the hydrophobic and hydrophilic fractions of the carbon surface. Moreover, a complex morphology  
19 of high surface area carbon particles, especially their porosity is not expected to facilitate the  
20 self-assembly, as Nafion® molecules, in spite of their flexibility, cannot follow all microstructural  
21 features of the carbon surface. Most likely, the factor determining Nafion® self-assembly is the  
22 graphitic fraction of the surface on the carbon particle perimeter. Consequently, it is rather the  
23 graphitic fraction of the “geometric” particle surface area, which is responsible for the  
24 self-assembly and oxygen confinement. The latter is believed to result from the oxygen affinity to  
25 the hydrophobic component of the ionomer, which is known to be predominantly responsible for  
26 the oxygen solubility in the polymer electrolyte.<sup>29</sup> However, the oxygen confinement may be  
27 enhanced by: (i) entrapment of O<sub>2</sub> molecules in the pores of carbon particles, (ii) a synergistic  
28 effect from the attractive interactions between the  $\pi$  electron rich graphene planes and oxygen  
29 molecules, and (iii) carbon surface curvature.  
30  
31  
32  
33  
34  
35  
36  
37  
38  
39  
40  
41  
42  
43  
44  
45  
46  
47  
48  
49  
50  
51  
52  
53  
54  
55  
56  
57  
58  
59  
60

1  
2  
3 The lack of any direct involvement of the metal centers of the macrocyclic complexes in the  
4 surface confinement of oxygen seems to contrast our previous conclusions regarding heat treated  
5 Fe/polyaniline composites.<sup>1</sup> A correlation between the surface density of the active sites and the  
6 amount of surface confined oxygen was detected by us for those catalysts and attributed to oxygen  
7 adsorption occurring either directly on the active sites or in their immediate vicinity. The disparity  
8 between the previous<sup>1</sup> and the current conclusions is most likely superficial. In reality, both results  
9 reflect the same phenomenon. As frequently postulated,<sup>3-5</sup> the FeN<sub>4</sub> active sites in pyrolyzed  
10 Fe/N/C composites are embedded in graphene planes and therefore their number is likely to  
11 correlate with the degree of surface graphitization. In turn, the latter is a key factor determining  
12 the extent of Nafion self-assembly and the resulting oxygen confinement, whereas the role of the  
13 very active sites in the reduction of surface confined oxygen is exclusively the electrochemical  
14 process, but not the adsorption itself. Such explanation of the previous results<sup>1</sup> remains in  
15 agreement with the insensitivity of the surface confinement of oxygen to the nature of the active  
16 site demonstrated in this paper.  
17  
18  
19  
20  
21  
22  
23  
24  
25  
26  
27  
28  
29  
30  
31  
32  
33  
34  
35

36 As previously noted,<sup>6</sup> the only active sites in a catalyst that can participate in ORR in the  
37 presence of Nafion® self-assembly are those with direct access to the electrolyte. Hydrophobic  
38 macrocyclic complexes, such as those used in the present study, likely adsorb exclusively on  
39 carbon graphitic planes<sup>30</sup> and are especially susceptible to blocking by the Nafion® hydrophobic  
40 component and to complete elimination from the electrocatalysis. Therefore, any ORR results  
41 obtained for Nafion® containing catalyst inks have to be first examined for possible Nafion®  
42 self-assembly, which may lead to a strong inhibition of the reaction but also to its apparent  
43 “acceleration” resulting from possible surface confinement of oxygen. The latter will not be visible  
44 in RRDE data obtained using a staircase methodology,<sup>1</sup> which allows for truly steady state  
45  
46  
47  
48  
49  
50  
51  
52  
53  
54  
55  
56  
57  
58  
59  
60

1  
2  
3 measurement. Catalyst supports such as graphitized carbons, graphene and carbon nanotubes are  
4  
5 expected to be especially susceptible to the inhibition and oxygen confinement phenomena  
6  
7  
8 originating from Nafion® self-assembly.  
9

#### 10 11 12 13 ACKNOWLEDGEMENTS 14

15  
16  
17 The financial support from the UC Office of the President (Lab Fees Research Program, grant  
18  
19 ID# 12-LR-237440) is gratefully acknowledged.  
20  
21  
22  
23  
24  
25  
26  
27  
28  
29  
30  
31  
32  
33  
34  
35  
36  
37  
38  
39  
40  
41  
42  
43  
44  
45  
46  
47  
48  
49  
50  
51  
52  
53  
54  
55  
56  
57  
58  
59  
60



1  
2  
3 REFERENCES  
4  
5  
6  
7  
8  
9  
10  
11  
12  
13  
14  
15  
16  
17  
18  
19  
20  
21  
22  
23  
24  
25  
26  
27  
28  
29  
30  
31  
32  
33  
34  
35  
36  
37  
38  
39  
40  
41  
42  
43  
44  
45  
46  
47  
48  
49  
50  
51  
52  
53  
54  
55  
56  
57  
58  
59  
60

1. Chlistunoff, J., RRDE and Voltammetric Study of ORR on Pyrolyzed Fe/Polyaniline Catalyst. On the Origins of Variable Tafel Slopes. *J. Phys. Chem. C* **2011**, *115*, 6496-6507.
2. Liu, Y., Is the Free Energy Change of Adsorption Correctly Calculated? *J. Chem. Eng. Data* **2009**, *54*, 1981-1985.
3. Lefevre, M.; Dodelet, J. P., Molecular Oxygen Reduction in Pem Fuel Cells: Evidence for the Simultaneous Presence of Two Active Sites in Fe-Based Catalysts. *J. Phys. Chem. B* **2002**, *106*, 8705-8713.
4. Koslowski, U. I.; Abs-Wurmbach, I.; Fiechter, S.; Bogdanoff, P., Nature of the Catalytic Centers of Porphyrin-Based Electrocatalysts for the ORR: A Correlation of Kinetic Current Density with the Site Density of Fe-N<sub>4</sub> Centers. *J. Phys. Chem. C* **2008**, *112*, 15356-15366.
5. Schulenburg, H.; Stankov, S.; Schünemann, V.; Radnik, J.; Dorbandt, I.; Fiechter, S.; Bogdanoff, P.; Tributsch, H., Catalysts for the Oxygen Reduction from Heat-Treated Iron(III) Tetramethoxyphenylporphyrin Chloride: Structure and Stability of Active Sites. *J. Phys. Chem. B* **2003**, *107*, 9034-9041.
6. Chlistunoff, J.; Sansiñena, J.-M., Nafion Effects on Oxygen Reduction Catalysis by Carbon Supported Transition Metal Macrocycles and Platinum. submitted to *J. Phys. Chem. C* **2015** (jp-2015-098636).
7. Hashe, F.; Oezaslan, M.; Strasser, P., Activity, Stability and Degradation of Multi Walled Carbon Nanotube (MWCNT) Supported Pt Fuel Cell Electrocatalysts. *PCCP* **2010**, *12*, 15251-15258.

- 1  
2  
3 8. Andersen, S. M.; Borghei, M.; Dhiman, R.; Jiang, H.; Ruiz, V.; Kauppinen, E.; Skou, E.,  
4 Interaction of Multi-Walled Carbon Nanotubes with Perfluorinated Sulfonic Acid Ionomers and  
5 Surface Treatment Studies. *Carbon* **2014**, *71*, 218-228.  
6  
7  
8  
9  
10  
11 9. Wang, G.; Sun, G.; Zhou, Z.; Liu, J.; Wang, Q.; Wang, S.; Guo, J.; Yang, S.; Xin, Q.; Yi,  
12 B., Performance Improvement in Direct Methanol Fuel Cell Cathode Using High Mesoporous  
13 Area Catalyst Support. *Electrochem. Solid-State Lett.* **2005**, *8*, A12-A16.  
14  
15  
16  
17  
18  
19 10. Garron, A.; Bennici, S.; Auroux, A., In Situ Generated Catalysts for  $\text{NabH}_4$  Hydrolysis  
20 Studied by Liquid-Phase Calorimetry: Influence of the Nature of the Metal. *Appl. Catalysis A:*  
21 *General* **2010**, *378*, 90-95.  
22  
23  
24  
25  
26  
27 11. Kinoshita, K., *Carbon: Electrochemical and Physicochemical Properties*; John Wiley &  
28 Sons: New York, NY, 1988.  
29  
30  
31  
32  
33 12. Pahalagedara, L.; Sharma, H.; Kuo, C. H.; Dharmarathna, S.; Joshi, A.; Suib, S.;  
34 Mhadeshwar, A. B. In *Influence of Particle Size and Microstructure on the Oxidation Behavior of*  
35 *Carbon Blacks and Diesel Soot*, 2012 AIChE Annual Meeting, Pittsburgh, PA, Pittsburgh, PA,  
36 2012; p 5.  
37  
38  
39  
40  
41  
42  
43 13. Ju, W.; Brulle, T.; Favaro, M.; Perini, L.; Durante, C.; Schneider, O.; Stimming, U.,  
44 *ChemElectroChem* **2015**, *2*, 547-558.  
45  
46  
47  
48  
49 14. Durst, J.; Siebel, A.; Simon, C.; Hashe, F.; Herranz, J.; Gasteiger, H. A., New Insights into  
50 the Electrochemical Hydrogen Oxidation and Evolution Reaction Mechanism. *Ener. Environ. Sci.*  
51 **2014**, *7*, 2255-2260.  
52  
53  
54  
55  
56  
57  
58  
59  
60

- 1  
2  
3 15. Durst, J.; Simon, C.; Hashe, F.; Gasteiger, H. A., Hydrogen Oxidation and Evolution  
4 Reaction Kinetics on Carbon Supported Pt, Ir, Rh, and Pd Electrocatalysts in Acidic Media. *J.*  
5  
6 *Electrochem. Soc.* **2015**, *162*, F190-F203.  
7  
8  
9  
10  
11 16. Guzman-Blas, R.; Suazo-Davila, D.; Velez, C. A.; Daza, C. E.; Stacchiola, D. J.; Sasaki,  
12  
13 K.; Senanayake, S. D.; Johnston-Peck, A. C.; Molina, R.; Cabrera, C. R., Edta-Ce(III) Modified  
14  
15 Pt Vulcan XC-72 Catalyst Synthesis for Methanol Oxidation in Acid Solution. *Electrocatalysis*  
16  
17 **2014**, *5*, 50-61.  
18  
19  
20  
21 17. Scherrer, P., Bestimmung Der Grösse Und Der Inneren Struktur Von Kolloidteilchen  
22  
23 Mittels Röntgenstrahlen. *Nachrichten von der Gesellschaft der Wissenschaften, Göttingen* **1918**,  
24  
25 98-100.  
26  
27  
28  
29 18. Laviron, E., General Expression of the Linear Potential Sweep Voltammogram in the Case  
30  
31 of Diffusionless Electrochemical Systems. *J. Electroanal. Chem.* **1979**, *101*, 19-28.  
32  
33  
34  
35 19. Nicholson, R. S.; Shain, I., Theory of Stationary Electrode Polarography. Single Scan and  
36  
37 Cyclic Methods Applied to Reversible, Irreversible, and Kinetic Systems. *Anal. Chem.* **1964**, *36*,  
38  
39 706-723.  
40  
41  
42  
43 20. Chlistunoff, J.; Pivovarov, B., Effects of Ionomer Morphology on Oxygen Reduction on Pt.  
44  
45 *J. Electrochem. Soc.* **2015**, *162*, F890-F900.  
46  
47  
48  
49 21. Ferreira-Aparicio, P.; Folgado, M. A.; Daza, L., High Surface Area Graphite as Alternative  
50  
51 Support for Proton Exchange Membrane Fuel Cell Catalysts. *J. Power Sources* **2009**, *192*, 57-62.  
52  
53  
54  
55 22. Coloma, F.; Sepulveda-Escribano, A.; Rodriguez-Roinoso, F., Heat-Treated Carbon  
56  
57 Blacks as Supports for Platinum Catalysts. *J. Catal.* **1995**, *154*, 299-305.  
58  
59  
60

1  
2  
3 23. Masuda, T.; Naohara, H.; Takakusagi, S.; Singh, P. R.; Uosaki, K., Formation and Structure  
4 of Perfluorosulfonated Ionomer Thin Film on a Graphite Surface. *Chem. Lett.* **2009**, *38*, 884-885.  
5  
6

7  
8  
9 24. Jiang, P.; Ma, X.; Ning, J.; Song, C.; Chen, X.; Jia, J.-F.; Xue, Q.-K., Quantum Size Effect  
10 Directed Selective Self-Assembling of Cobalt Phthalocyanine on Pb(111) Thin Films. *J. Am.*  
11 *Chem. Soc.* **2008**, *130*, 7790-7791.  
12  
13  
14

15  
16  
17 25. Artyushkova, K.; Pylypenko, S.; Dowlapalli, M.; Atanassov, P., Structure-to-Property  
18 Relationships in Fuel Cell Catalyst Supports: Correlation of Surface Chemistry and Morphology  
19 with Oxidation Resistance of Carbon Blacks. *J. Power Sources* **2012**, *214*, 303-313.  
20  
21  
22

23  
24  
25 26. Ohma, A.; Fushinobu, K.; Okazaki, K., Influence of Nafion® Film on Oxygen Reduction  
26 Reaction and Hydrogen Peroxide Formation on Pt Electrode for Proton Exchange Membrane Fuel  
27 Cell. *Electrochim. Acta* **2010**, *55*, 8829-8838.  
28  
29  
30

31  
32  
33 27. Kangasniemi, K. H.; Condit, D. A.; Jarvi, T. D., Characterization of Vulcan  
34 Electrochemically Oxidized under Simulated Pem Fuel Cell Conditions. *J. Electrochem. Soc.*  
35 **2004**, *151*, E125-E132.  
36  
37  
38

39  
40  
41 28. Paul, D. K.; Karan, K.; Docoslis, A.; Giorgi, J. B.; Pearce, J., Characteristics of Self-  
42 Assembled Ultrathin Nafion Films. *Macromolecules* **2013**, *46*, 3461-3475.  
43  
44

45  
46  
47 29. Evans, C. M.; Singh, M. R.; Lynd, N. A.; Segalman, R. A., Improving the Gas Barrier  
48 Properties of Nafion Via Thermal Annealing: Evidence for Diffusion through Hydrophilic  
49 Channels and Matrix. *Macromolecules* **2015**, *48*, 3303-3309.  
50  
51  
52

- 1  
2  
3 30. Kozub, B. R.; Compton, R. G., Voltammetric Studies of the Redox Mediator, Cobalt  
4 Phthalocyanine, with Regard to Its Claimed Electrocatalytic Properties. *Sensors and Actuators B*  
5  
6 **2010**, *147*, 350-358.  
7  
8  
9  
10  
11  
12  
13  
14  
15  
16  
17  
18  
19  
20  
21  
22  
23  
24  
25  
26  
27  
28  
29  
30  
31  
32  
33  
34  
35  
36  
37  
38  
39  
40  
41  
42  
43  
44  
45  
46  
47  
48  
49  
50  
51  
52  
53  
54  
55  
56  
57  
58  
59  
60

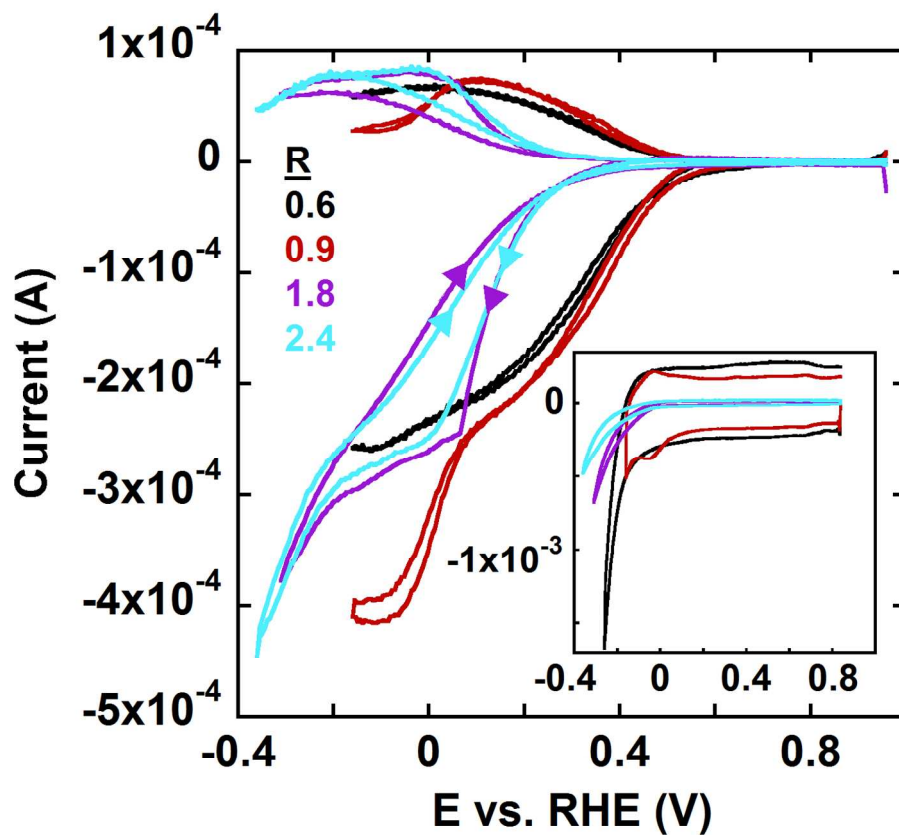


Figure 1. Background corrected RRDE voltammograms of oxygen saturated  $0.5 \text{ mol dm}^{-3} \text{ H}_2\text{SO}_4$  solution recorded for a 5.7% CoPC on Vulcan XC72. Total carbon loading 0.1 mg. Rotation rate 400 rpm. Scan rate  $10 \text{ mV s}^{-1}$ . Nafion® contents (R) in the catalyst inks listed in the figure. Inset: cyclic voltammograms ( $100 \text{ mV s}^{-1}$ ) recorded for the same catalysts in deoxygenated  $0.5 \text{ mol dm}^{-3} \text{ H}_2\text{SO}_4$  solutions.

190x190mm (216 x 216 DPI)

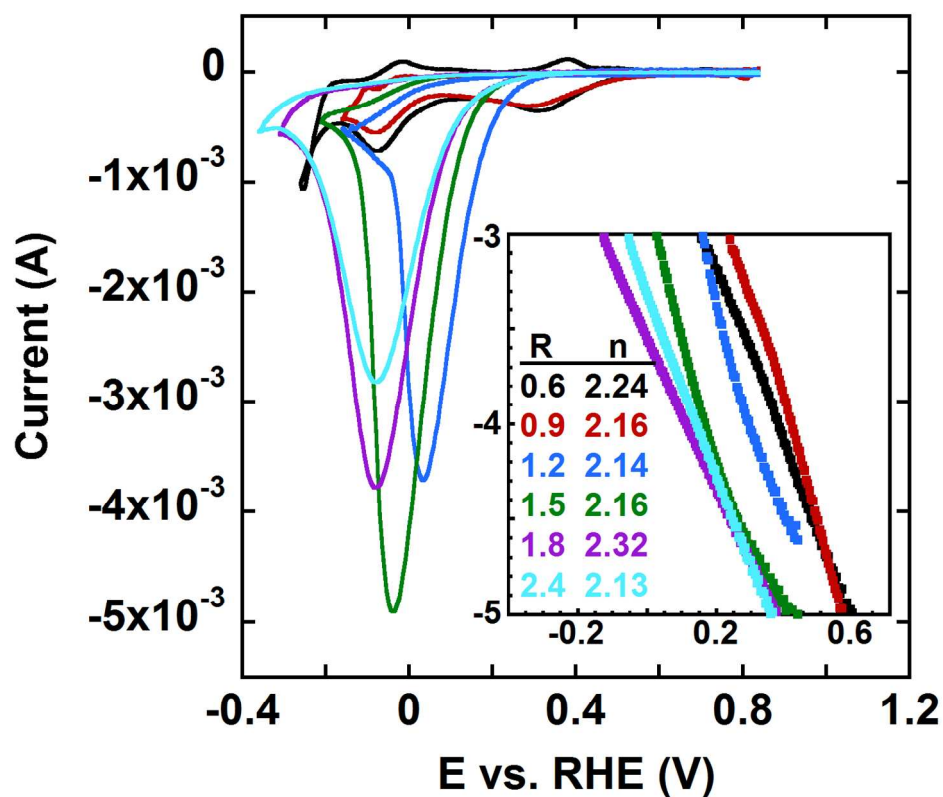


Figure 2. Cyclic voltammograms of oxygen saturated  $0.5 \text{ mol dm}^{-3} \text{ H}_2\text{SO}_4$  solution recorded for a 5.7% CoPC on Vulcan XC72. Total carbon loading 0.1 mg. Scan rate  $500 \text{ mV s}^{-1}$ . Equilibration time 5 min at 400 rpm.

Nafion® contents in the catalyst inks listed in the figure. Inset: kinetic ORR currents determined for the same catalysts from RRDE experiments at 400 rpm. Nafion® contents (R) in the catalyst inks and the respective numbers of electrons (n) transferred in ORR listed in the figure.

192x190mm (216 x 216 DPI)

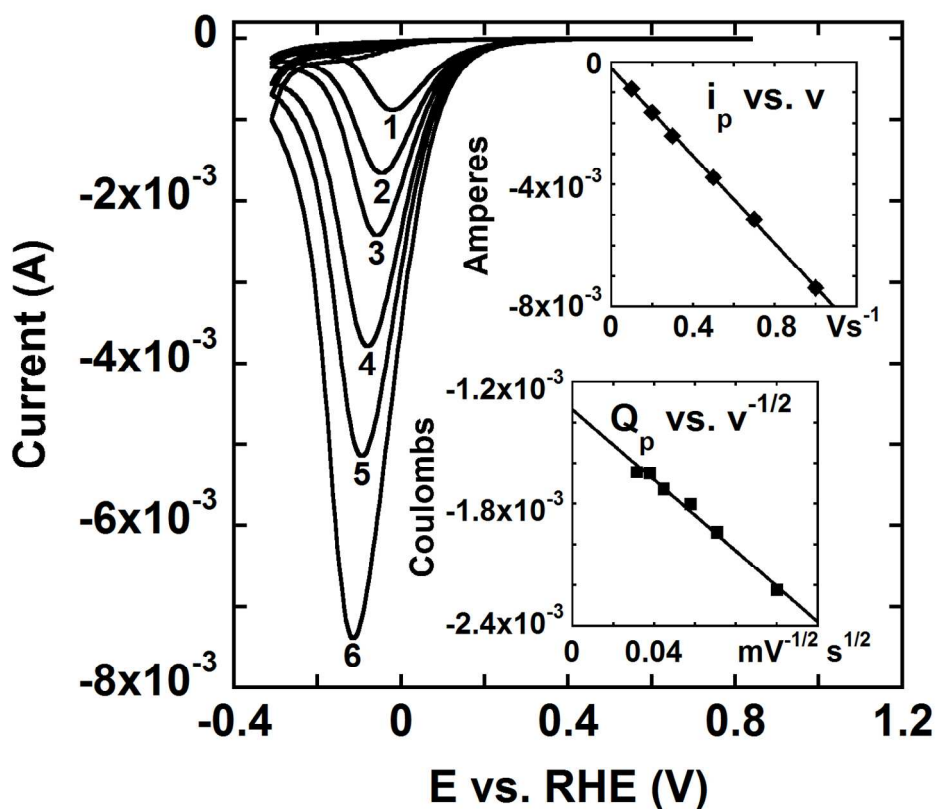


Figure 3. Cyclic voltammograms of oxygen saturated 0.5 mol dm<sup>-3</sup> H<sub>2</sub>SO<sub>4</sub> solution recorded for 5.7% CoPC on Vulcan XC72. Total carbon loading 0.1 mg. Equilibration time 5 min at 400 rpm. R = 1.8. Scan rate (mV s<sup>-1</sup>): 100 (1), 200 (2), 300 (3), 500 (4), 700 (5), 1000 (6). Top inset: peak current vs. scan rate. Bottom inset: oxygen reduction charge plotted vs. inverse square root of the scan rate (see text for the charge determination methodology).  
190x190mm (216 x 216 DPI)



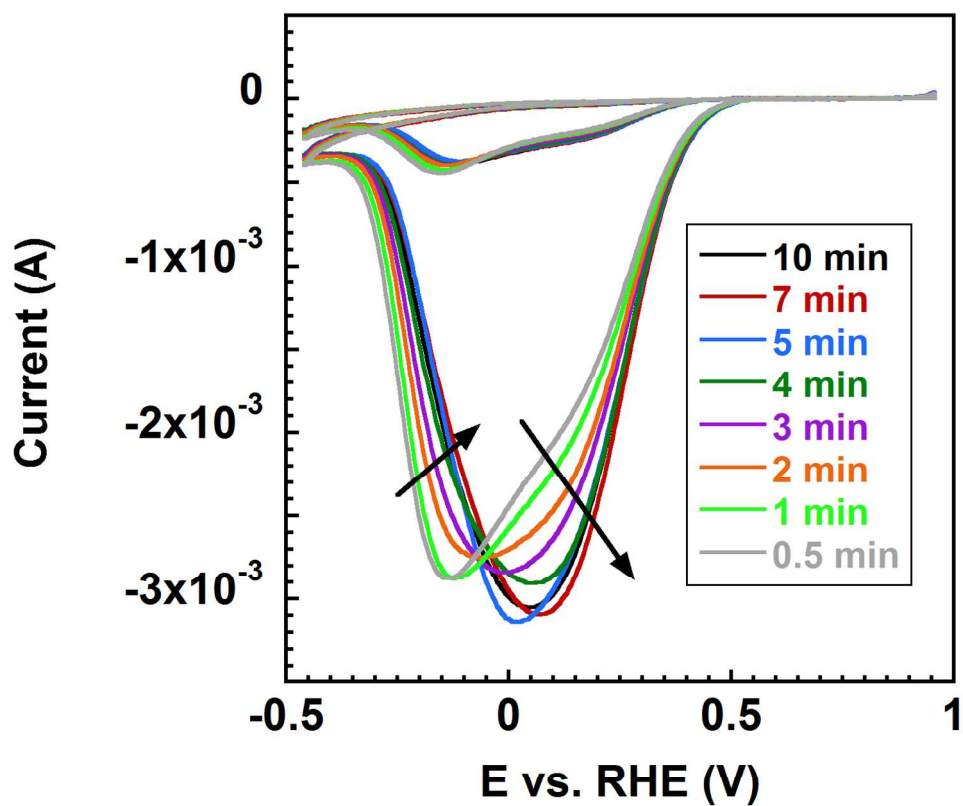


Figure 4. Two cycle voltammograms of oxygen saturated  $0.5 \text{ mol dm}^{-3} \text{ H}_2\text{SO}_4$  solution recorded for 8.1% CoTPP on Vulcan XC72 after different equilibration times at 400 rpm. Total carbon loading 0.1 mg.  $R = 1.6$ . Scan rate  $1000 \text{ mV s}^{-1}$ . 190x190mm (216 x 216 DPI)

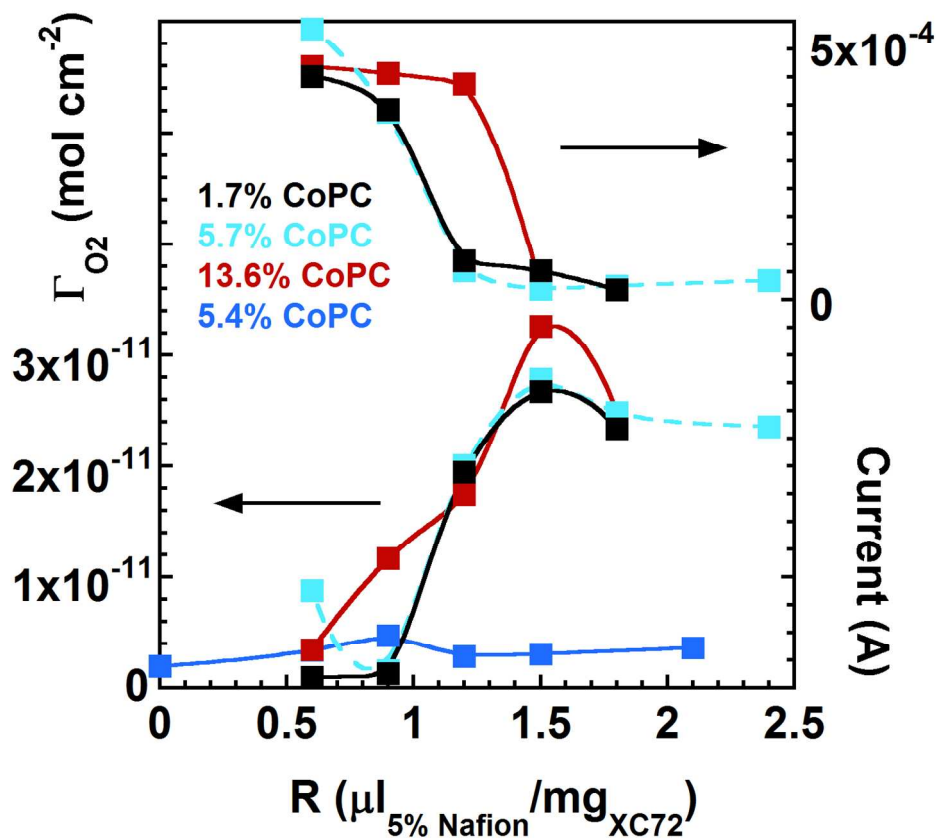


Figure 5. Oxygen surface concentrations (bottom) and voltammetric background currents measured at 0.3 V vs. RHE and  $100 \text{ mV s}^{-1}$  (top) plotted against Nafion® content (R) in the catalyst layer. The background currents are sums of absolute currents measured in negative and positive scans. For the 5.4% CoPC catalyst, Nafion® was deposited on top of the Nafion® free catalyst layer as an aqueous solution obtained by 100-fold dilution of the commercial 5% solution.

190x190mm (216 x 216 DPI)

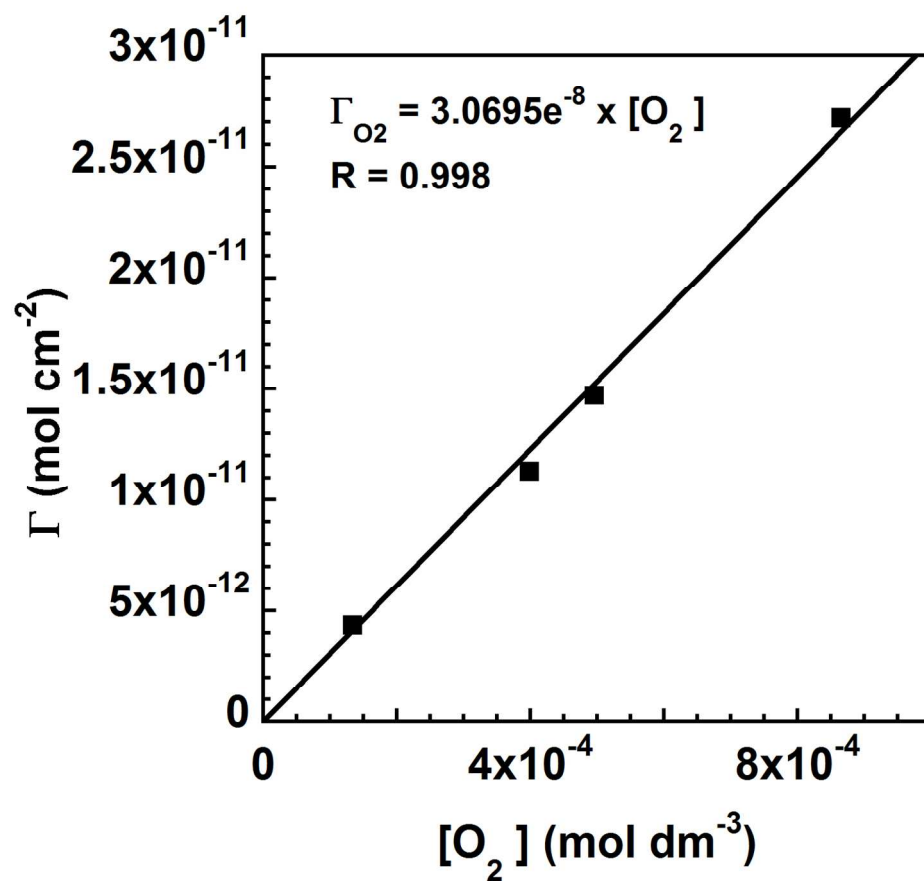


Figure 6. Oxygen adsorption isotherm for 8.1% CoTPP catalyst ( $R = 1.6$ ) in  $0.5 \text{ mol dm}^{-3} \text{ H}_2\text{SO}_4$  solution. 190x190mm (216 x 216 DPI)

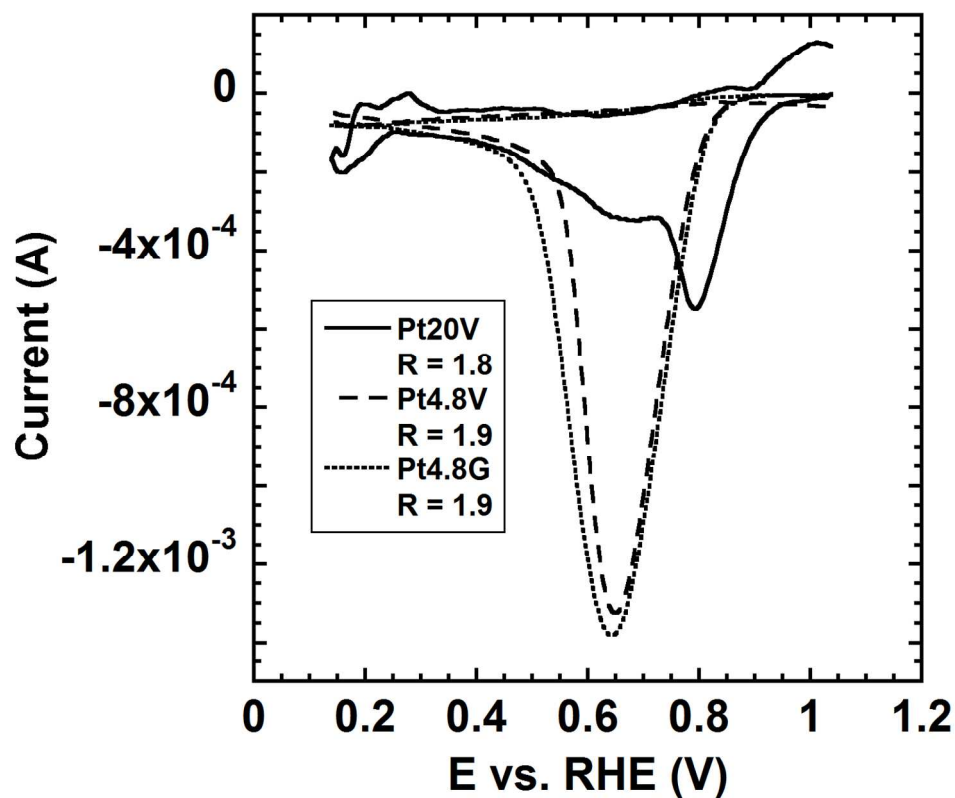


Figure 7. Background corrected cyclic voltammograms of oxygen saturated  $0.5 \text{ mol dm}^{-3} \text{ H}_2\text{SO}_4$  solution recorded for three Pt catalysts after 5 min equilibration at 400 rpm. Scan rate  $100 \text{ mV s}^{-1}$ . Nafion® contents in the catalyst layers listed in the legend.  
190x190mm (216 x 216 DPI)

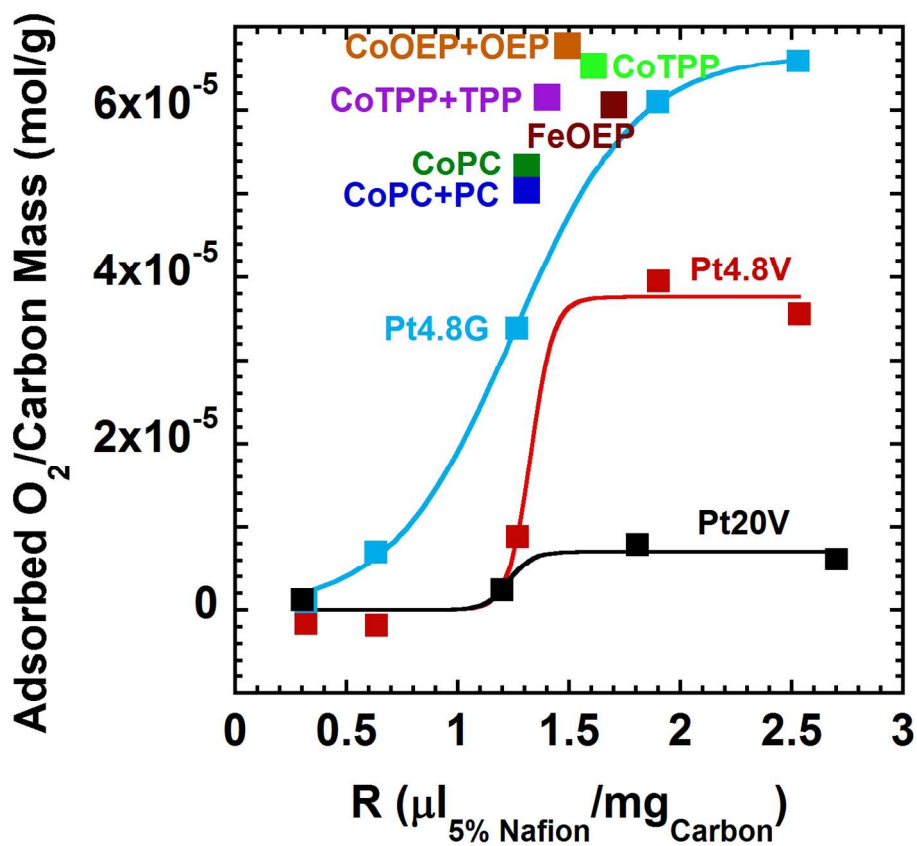


Figure 8. Molar concentrations of surface confined oxygen per gram of catalyst support in oxygen saturated  $0.5 \text{ mol dm}^{-3} \text{ H}_2\text{SO}_4$  solution plotted against Nafion® content in the catalyst layer for three Pt catalysts on different carbon supports and six macrocyclic complexes of Co and iron supported on Vulcan XC72.

Macrocyclic catalyst compositions: CoPC (6.4%), CoPC + PC (5.0% CoPC, 5.0% PC), FeOEP (9.8% FeOEP), CoTPP (8.1%), CoTPP + TPP (6.0% CoTPP, 6.2% TPP), CoOEP + OEP (6.9% CoOEP, 6.5% OEP).  
190x190mm (216 x 216 DPI)

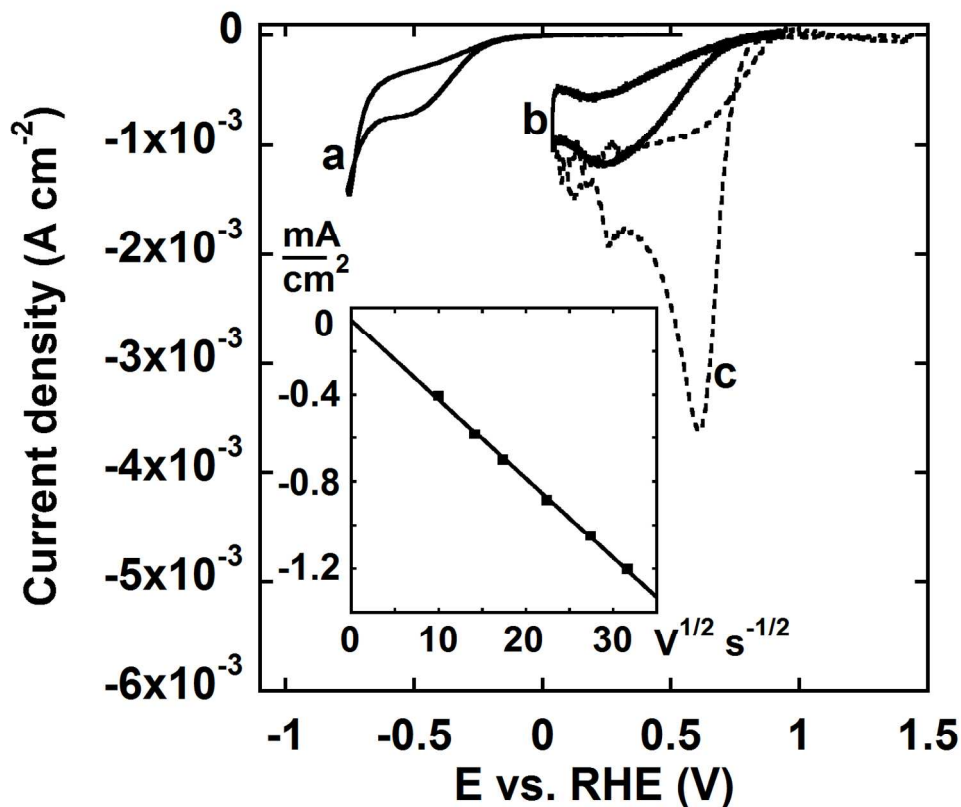


Figure 9. Background corrected cyclic voltammograms of oxygen saturated 0.5 mol dm<sup>-3</sup> H<sub>2</sub>SO<sub>4</sub> solution recorded for 2 × 10<sup>-9</sup> mol cm<sup>-2</sup> CoPC (a) and Pt nanoparticles (0.024 cm<sup>2</sup> surface area, b) deposited on ~4.8 mm HOPG disk and covered with a self assembled Nafion® film as well as for an uncoated 1.6 mm Pt disk. Scan rate 1 V s<sup>-1</sup>. Inset: peak current density for the HOPG/Pt/Nafion® electrode plotted against the square root of scan rate.

190x190mm (216 x 216 DPI)

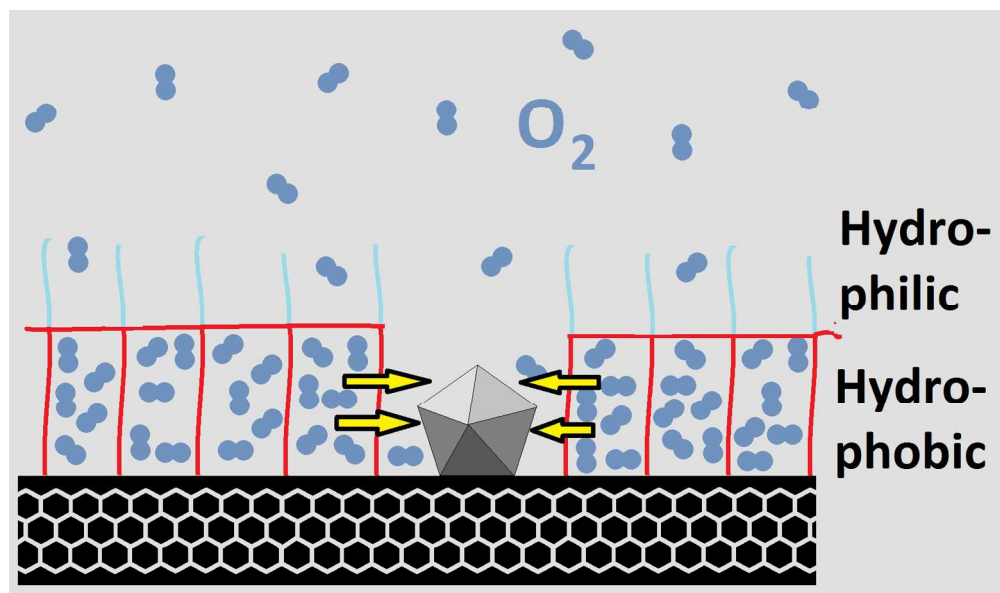


Table of content graphics  
473x278mm (96 x 96 DPI)